Dynamic Hopf Bifurcation in Spatially Extended Excitable Systems from Neuroscience

by

Lydia M. Bilinsky

A Dissertation Presented in Partial Fulfillment
of the Requirements for the Degree
Doctor of Philosophy

Approved November 2012 by the
Graduate Supervisory Committee:

Steven M. Baer, Chair
Sharon M. Crook
Zdzislaw Jackiewicz
Carl L. Gardner
Ranu Jung

ARIZONA STATE UNIVERSITY

December 2012

ABSTRACT

One explanation for membrane accommodation in response to a slowly rising current, and the phenomenon underlying the dynamics of elliptic bursting in nerves, is the mathematical problem of dynamic Hopf bifurcation. This problem has been studied extensively for linear (deterministic and stochastic) current ramps, nonlinear ramps, and elliptic bursting. These studies primarily investigated dynamic Hopf bifurcation in space-clamped excitable cells. In this study we introduce a new phenomenon associated with dynamic Hopf bifurcation. We show that for excitable spiny cables injected at one end with a slow current ramp, the generation of oscillations may occur an order one distance away from the current injection site. The phenomenon is significant since in the model the geometric and electrical parameters, as well as the ion channels, are uniformly distributed. In addition to demonstrating the phenomenon computationally, we analyze the problem using a singular perturbation method that provides a way to predict when and where the onset will occur in response to the input stimulus. We do not see this phenomenon for excitable cables in which the ion channels are embedded in the cable membrane itself, suggesting that it is essential for the channels to be isolated in the spines.

ACKNOWLEDGEMENTS

I would like to thank my advisor, Dr. Steven M. Baer, for his outstanding guidance and support during this research. I would also like to thank Drs. Sharon Crook, Ranu Jung, Zdzislaw Jackiewicz, and Carl Gardner for their invaluable expertise.

TABLE OF CONTENTS

CHAPTER Page

CHAPTER Page

LIST OF FIGURES

Chapter 1

INTRODUCTION

1.1 Membrane accommodation and dynamic Hopf bifurcation

Nerve membrane exhibits a property known as excitability: a constant injected current elicits sustained, large-amplitude oscillations in the membrane electrical potential provided that the current falls into a specific range $[I_L, I_U]$, called the firing range. In 1849 Emil du Bois-Reymond found that injecting a nerve fiber with a very slowly rising current ramp raises the firing threshold [7]. In 1908 Walther Hermann Nernst named this phenomenon "accommodation" [21]. In 1964, Vallbo [28] demonstrated the existence of a minimal ramp speed (increase in current per unit time) below which certain excitable tissues will not fire, no matter how large the value of injected current becomes; I refer to this situation as "complete accommodation."

In 1952, Hodgkin and Huxley published a mathematical model of an excitable nerve fiber developed from their experiments with the squid giant axon, which established that the phenomenon of excitability is caused by the opening and closing of voltage-gated ion channels embedded in the nerve membrane [11]. In the standard Hodgkin-Huxley model, as well as the simpler FitzHugh-Nagumo model [9], there exists an interval $I_1 < I < I_2$ for repetitive spiking, where I_1 and I_2 denote Hopf bifurcations. At a Hopf point, there is an abrupt onset of repetitive spiking at a nonzero firing frequency. This is called type 2 dynamics [27]. Hence, for Hodgkin-Huxley-like excitable systems, with type 2 dynamics, the transition through the constant-current firing threshold by means of a slow current ramp is mathematically a case of slow passage through a Hopf bifurcation, also known as "dynamic Hopf

bifurcation."

The problem of dynamic Hopf bifurcation has been investigated by many authors; for early theoretical treatments see [20] and [14]. Baer, Erneux and Rinzel [1] took a different approach and applied the WKB (Wentzel, Kramers, and Brillouin) method, a technique for obtaining an asymptotic expansion for the solution to a linear homogeneous differential equation with slowly-varying coefficients [4]. These authors obtained the following result. Suppose that one has an analytic system with constant parameter I which undergoes a Hopf bifurcation at $I = I_H$, such that for $I < I_H$ the steady state is asymptotically stable. Then if I is not constant but instead made to slowly vary according to $I(t) = I_0 + \epsilon t$, where $I_0 < I_H$ and the ramp speed $\epsilon > 0$ is very small, then the onset of large-amplitude oscillations will not occur as soon as I attains I_H, but will be delayed by some amount of time, and appear at $I_j > I_H$. This phenomenon persists no matter how small the ramp speed ϵ becomes: as $\epsilon \to 0$, I_j does not approach I_H.

The problem of determining the apparent firing threshold I_j is a singular perturbation problem with small parameter ϵ, the ramp speed; this is why I_j does not approach the static firing threshold I_H as $\epsilon \to 0$. The formula specifying I_j as a function of initial current I_0 (the "onset condition") was derived by Baer, Erneux and Rinzel in [1] for the FitzHugh-Nagumo model subjected to a slow linear current ramp. The onset condition dictates that the further back I_0 begins from I_H, the larger will be the value I_j at which the system actually loses stability; this was called the "memory effect" [1]. In [2] Baer and Gaekel considered slow monotonic current ramps of general functional form and found that "accelerating ramps" such as $I = I_0 + (\epsilon t)^2$ result in a firing threshold exceeding that for a linear ramp, while "decelerating

ramps" such as $I = I_0 + \sqrt{\epsilon t}$ result in a lower firing threshold than for a linear ramp.

Dynamic Hopf bifurcation is the proposed mechanism underlying elliptic bursting, a firing pattern seen "in thalamic neurons, rodent trigeminal neurons, and certain neurons found in the basal ganglia" [8]. It also arises elsewhere in nature; for example, it is the proposed mechanism underlying the spontaneous formation of targets in the unstirred Belousov-Zhabotinsky (BZ) chemical reaction [10, 24].

1.2 Previous results on dynamic Hopf bifurcation in excitable systems from neuroscience

The first investigation of dynamic Hopf bifurcation in a model of an excitable cell was Jakobsson and Guttman, 1980 [12], followed by Rinzel and Baer in 1988 [22]. In 1989, Baer, Erneux and Rinzel investigated the space-clamped (no spatial extension) FitzHugh-Nagumo model subjected to a slowly rising linear current ramp $I = I_0 + \epsilon t$, $\epsilon \to 0$. They found that in general the apparent firing threshold I_j exceeds the the constant-current firing threshold given by the first Hopf point of the system [1]. In [2] Baer and Gaekel investigated the FitzHugh-Rinzel model of elliptic bursting, in which the slow subsystem describing the evolution of the current variable is bidirectionally coupled to the FitzHugh-Nagumo fast subsystem. Dynamic Hopf bifurcation is responsible for the alternation between silent and bursting phases in this model. Baer and Gaekel noted that during the silent phase, the time course of the current is of the form of a slow monotonic ramp, not necessarily linear, and derived an onset condition to compute the duration of the silent phase; these estimates were in excellent agreement with numerical solutions. Su [25] investigated the

response of a FitzHugh-Nagumo cable with sealed ends to a non-uniform linear current ramp applied transversally to the entire cable membrane (the current density varied over the length of the cable) and found that the delay effect still holds.

An apparent counterexample to the delay effect was described in [12] by Jakobsson and Guttman. They found that numerical solutions of the space-clamped Hodgkin-Huxley model fail to accommodate to a slow linear current ramp for very small ramp speeds. The apparent firing threshold initially increases with decreasing ramp speed, consistent with the delay effect, but as the ramp speed is further reduced the apparent firing threshold comes down again; this same trend was seen in physical experiments on squid axon injected with a linear current ramp. In [22] and [1] Baer, Erneux and Rinzel showed that this apparent counterexample is due to roundoff error resulting from the very large number of time steps needed to simulate a slow current ramp. Jakobsson and Guttman used single precision arithmetic; when double precision was used, numerical results consistent with the delay effect persisted for much smaller values of the ramp speed. However, noise is present in physical systems such as axons, in part due to fluctuations in conductances caused by the opening and closing of ion channels, explaining the failed accommodation in the squid axon for very small ramp speeds [22]. The impact of noise on dynamic Hopf bifurcation is important, and treatments of this can be found in [17, 18, 26]. Here, I restrict myself to a deterministic study and execute all numerical solutions in quadruple precision arithmetic to minimize the issue of roundoff error.

1.3 Main result of this work

With the exception of Su [25], previous work on dynamic Hopf bifurcation has focused on systems with no spatial structure, for example, an ordinary differential equation model of an isopotential excitable cell. In the present work I investigate dynamic Hopf bifurcation in some spatially extended excitable systems from neuroscience. The first system I consider models a dendritic shaft that has only passive electrical properties, but which is studded with excitable dendritic spines, tiny evaginations of the dendritic membrane. Dendritic spines consist of a bulbous "head" attached to the shaft by means of an elongated "neck" [3, 23]. I refer to this model as the spiny cable. The second system I consider models an excitable nerve fiber such as an axon in which the channels responsible for excitability are embedded in the membrane; I refer to this as an axonal cable. For each system, I investigate the response to a slowly rising current ramp injected into one end of the cable while the other end is sealed to current. I note the difference here from Su's investigations: here, I model a situation in which current is injected into one end of the cable while the other end is sealed, while Su studied a model in which a nonuniform current density was applied over the cable's surface and both ends were sealed.

My main result is as follows: isolating the ion channels in spineheads can cause the oscillations in membrane potential that arise at the onset of instability to occur at a location along the cable which is quite distal from the current injection site; in particular, the greater the amount by which the apparent firing threshold exceeds the constant-current firing threshold (the first Hopf point), the farther from the injection end of the cable will the oscillations arise. Both the spiny and axonal cables show the firing-threshold memory ef-

fect, but only the spiny cable shows distal initiation of oscillations. This result holds even for a uniform cable studded with identical, uniformly distributed spines with uniform stem conductances, and in response to a linear current ramp. Following the earlier work of Baer, Erneux and Rinzel, I obtained the apparent firing threshold I_j via the WKB method, and found that the WKB method provides not only I_j, but also with the location along the cable at which oscillations arise once I_j is attained.

With the exception of the simple ODE model considered in chapter two, all models considered are partial differential equations. For the spiny cable, I used a modified version of the PDE model due to Baer and Rinzel [3], in which the spines are treated as a continuum. Although spines are discrete, Baer and Rinzel found that this approximation is good for sufficiently large spine density. For both the spiny and axonal cables, I wrote an approximating ODE system which was obtained by viewing the cable as consisting of a large number of isopotential compartments, and it is to this approximating ODE system that I applied the WKB method. All WKB predictions were compared with numerical solutions of the actual PDE equation obtained via finite difference methods.

The thesis is organized as follows. In chapter two I consider a model of a passive cable with two excitable FitzHugh-Nagumo spines, each located at one end of the cable. I inject a slow current ramp into one end of the cable and seal the other end to current. I make the simplifying assumption that the potential in the cable evolves on a much faster time scale than the dynamics in the spineheads, so that at each instant of time the cable potential is what it would be if the spinehead potentials were held constant at their instantaneous values; this is known as the quasi-static approximation, and I refer to such a

model as the "reduced model," in contrast to the "full model" [18,30,31]. This reduced model of a passive cable with two excitable spines is a very simple excitable system featuring spatial extension, and I demonstrate the ability of the WKB method to determine in which spine oscillations in potential arise when the apparent firing threshold is reached. In chapter three I investigate the response to a slow current ramp of a passive cable studded with a large number of excitable FitzHugh-Nagumo spines; here I do not make the quasi-static approximation. In chapter four I investigate the response of FitzHugh-Nagumo and Hodgkin-Huxley axonal cables to a slow current ramp. In chapter five I review my findings and consider possible implications and directions for further work.

Chapter 2

TWO FITZHUGH-NAGUMO SPINES COUPLED VIA A PASSIVE CABLE

2.1 Review of results for the space-clamped FitzHugh-Nagumo model injected with a slowly rising current ramp

The FitzHugh-Nagumo model of nerve excitability features two dependent variables. u represents membrane potential, and w is a slow recovery variable which serves to return u to its resting value. A review of the FitzHugh-Nagumo model is given in the Appendix. Baer, Rinzel and Erneux [1] investigated the response of the FitzHugh-Nagumo model to a slow linear current ramp $I(t) = I_0 + \epsilon t$ and used the WKB method to derive the onset condition, which gives the apparent firing threshold as a function of the initial current I_0 in the limit $\epsilon \to 0$. By "apparent firing threshold" I mean the value of injected current at the moment large-amplitude oscillations in the u variable, representing membrane potential, appear. Baer and Gaekel [2] extended the onset condition to the case of general monotonic current ramps. A detailed derivation of the onset condition for a linear current ramp and a description of the FitzHugh-Nagumo model can be found in the Appendix. Here I summarize the key points.

When injected current I is constant, the FitzHugh-Nagumo model has a unique steady state (for the parameters I use, given in the Appendix) which is a function of the injected current. To determine the firing threshold, one linearizes about the steady state and determines the value of I at which it changes from being stable to unstable, as indicated by an eigenvalue attaining positive real part. This occurs at the lower Hopf point I_H; hence, I_H is the

firing threshold in response to a constant current.

When the injected current is a slowly-varying function of time, there is no longer a steady state, but there is an analogue to it which is called the slowly-varying solution. The slowly-varying solution stays close to the constant-current steady state viewed as a function of I. In order to determine the value of I at which firing commences, one must linearize about the slowly-varying solution. This yields a linear homogeneous differential equation with time-varying coefficients and small parameter ϵ multiplying the highest-order derivative. Assuming the WKB expansion for the solution, one obtains the following onset condition [2]: in the limit that ramp speed $\epsilon \to 0$, large-amplitude oscillations will be evoked by a monotonic current ramp $I(t) = I_0 + g(\epsilon t)$ when the current attains the value I_j, where I_j is the smallest current value satisfying

$$\int_{I_0}^{I_j} [g^{-1}(I - I_0)]' Re(\lambda(I)) dI = 0 \tag{2.1}$$

for some eigenvalue $\lambda(I)$. As detailed in the Appendix, the eigenvalues referenced in the onset condition are eigenvalues of the Jacobian of the system with constant current evaluated at the steady state. As I varies, so does the constant-current steady state; hence, the eigenvalues are functions of I.

One can see that the apparent firing threshold I_j depends on the initial current I_0 as well as the shape of the ramp, as dictated by g. For a linear ramp, the onset condition simplifies to

$$\int_{I_0}^{I_j} Re(\lambda(I)) dI = 0. \tag{2.2}$$

One can understand the onset condition intuitively by considering that during

dynamic Hopf bifurcation, time is spent winding in to the slowly-varying solution when I is in the range $[I_0, I_H]$. Once $I > I_H$, the solution starts winding out. For large-amplitude oscillations to appear, the solution must first wind out by the same amount that it has wound in; I_j is the value of the current at the moment this occurs.

The 2-variable FitzHugh-Nagumo model lacks spatial extension. I now consider a very simple spatially extended excitable system, dealt with by [31] in her studies of its response to constant injected current. I find that the WKB method can be used to determine not just the apparent firing threshold in response to a slow current ramp, but also where the large-amplitude oscillations will arise.

2.2 Two FitzHugh-Nagumo spines coupled via a passive cable, with slow current ramp injected at one end

Consider a model of a segment of passive dendritic cable to which are attached two excitable dendritic spines, one at either end. I model the spines as obeying FitzHugh-Nagumo dynamics, and the cable as obeying the passive cable equation. Suppose that one injects a slow current ramp $I = I_0 + \epsilon t$ into one end of the cable and seals the other end to current. No current is applied directly to the spines. Let the spine at the end of the cable where current is injected have stem conductance Gss_1, and let the stem conductance for the other spine be Gss_2; here I ignore the cable properties of the spine stems and model them as a lumped Ohmic resistance. This system obeys the following equations:

$$\frac{\tau \partial V}{\partial t} = \frac{\partial^2 V}{\partial X^2} - V \tag{2.3}$$

$$\frac{du_1}{dt} = -f(u_1) - w_1 - G_{ss1}(u_1 - V(0,t)) \tag{2.4}$$

$$\frac{dw_1}{dt} = b(u_1 - \gamma w_1) \tag{2.5}$$

$$\frac{du_2}{dt} = -f(u_2) - w_2 - G_{ss2}(u_2 - V(L,t)) \tag{2.6}$$

$$\frac{dw_2}{dt} = b(u_2 - \gamma w_2) \tag{2.7}$$

with boundary conditions

$$\frac{\partial V(0,t)}{\partial X} = -R_\infty (I(t) + G_{ss1}(u_1 - V(0))) \tag{2.8}$$

$$\frac{\partial V}{\partial X}(L,t) = R_\infty G_{ss2}(u_2 - V(L)). \tag{2.9}$$

The boundary conditions are statements of conservation of current at the two ends of the cable. Here, R_∞ is defined as

$$R_\infty = \lambda \frac{R_i}{\pi d^2/4} \tag{2.10}$$

$$= (2/\pi)\sqrt{R_i R_m / d^3}. \tag{2.11}$$

In the system equations and boundary conditions, λ is the space constant for the cable (not to be confused with the eigenvalues), τ is the time constant for the cable, d is the cable diameter, R_i is the axial resistivity of the cable, and R_m is the transverse resistivity of the cable. Here, I have nondimensionalized the cable equation with respect to space but not time. That is, the length X is the electrotonic length, equal to the physical length x divided by the cable space constant λ, while time is measured in seconds.

Reduced model obtained via the quasi-static approximation

If b is small in the FitzHugh-Nagumo equations then the potential in the spineheads undergoes relaxation oscillations and for most of the time changes on a much slower time scale than does the potential in the cable [18, 30, 31]. Then one is justified in using the quasi-static approximation, in which one approximates at each point in time the potential in the cable $V(X,t)$ as being at the steady state $V_s(X)$ that would eventually be reached if the spinehead potentials were held constant at their values at time t, $u_1(t)$ and $u_2(t)$; for a detailed explanation and examples of the quasi-static approximation, see [18, 30, 31]. Then one can replace the above partial differential equation with an ordinary differential equation:

$$\begin{aligned}
\frac{du_1}{dt} &= -f(u_1) - w_1 - G_{ss1}(u_1 - V_s(0)) && (2.12)\\
\frac{dw_1}{dt} &= b(u_1 - \gamma w_1) && (2.13)\\
\frac{du_2}{dt} &= -f(u_2) - w_2 - G_{ss2}(u_2 - V_s(L)) && (2.14)\\
\frac{dw_2}{dt} &= b(u_2 - \gamma w_2). && (2.15)
\end{aligned}$$

One must compute $V_s(X)$. Suppose that the potentials in the spineheads at time t are u_1 and u_2. Then

$$V_s(X) = A\cosh X + B\sinh X \tag{2.16}$$

where A and B are constants depending on u_1 and u_2, and determined from the boundary conditions. One has that

$$
\begin{aligned}
V_s(0) &= A && (2.17)\\
\frac{\partial V_s}{\partial X}(0) &= B && (2.18)\\
V_s(L) &= A\cosh L + B\sinh L && (2.19)\\
\frac{\partial V_s}{\partial X}(L) &= A\sinh L + B\cosh L && (2.20)
\end{aligned}
$$

and from the boundary conditions,

$$
\begin{aligned}
\frac{\partial V_s}{\partial X}(0) &= -R_\infty(I + G_{ss1}(u_1 - V_s(0))) && (2.21)\\
\frac{\partial V_s}{\partial X}(L) &= R_\infty G_{ss2}(u_2 - V_s(L)). && (2.22)
\end{aligned}
$$

Combining these equations, one obtains the following equations relating A and B to u_1 and u_2:

$$-R_\infty(I(t) + G_{ss1}u_1) = -R_\infty G_{ss1}A + B \quad (2.23)$$

$$R_\infty G_{ss2}u_2 = (\sinh L + R_\infty G_{ss2}\cosh L)A + (\cosh L + R_\infty G_{ss2}\sinh L)B. \quad (2.24)$$

$V_s(0)$ and $V_s(L)$ are linear combinations of u_1, u_2, and the applied dendritic current $I(t)$. Hence, equations (2.12-2.16, 2.23-2.24) constitute a well-defined ODE in the four spinehead variables, and one may abandon explicit reference to the cable variables. I shall refer to this system, obtained by the quasi-static approximation, as the "reduced model" [18,30,31], in contrast to the full model of equations (2.3-2.9).

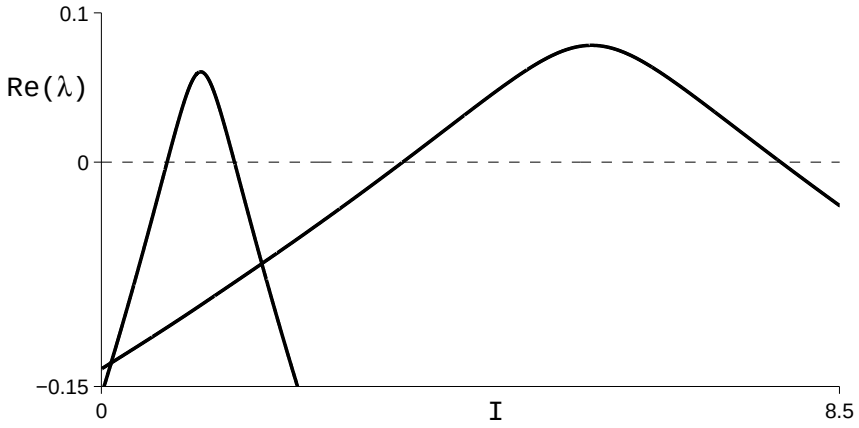

Figure 1: $G_{ss1} = 0.05$, $G_{ss2} = 0.01$. $Re(\lambda(I))$ versus I for the four eigenvalues associated with the system.

Numerical solutions of reduced model and WKB prediction for I_j

The two-spine system has four variables and hence four eigenvalues for each value of I. As discussed in the Appendix, when there are several eigenvalues attaining positive real part for some I, the prediction for the apparent firing threshold is the smallest $I_j > I_0$ such that the onset condition is satisfied for one of the eigenvalues. Figure 1 shows the real portions of the four eigenvalues (two complex-conjugate pairs) as a function of I for the $L = 0.5$ cable with stem conductances $G_{ss1} = 0.05$, $G_{ss2} = 0.01$. Figure 2 shows the WKB prediction for I_j in response to the slow ramp $I(t) = 0.5 + \epsilon t$. I_j is such that the signed area under the graph of $Re(\lambda(I))$ (shown shaded) between $I = I_0 = 0.5$ and $I = I_j$ is zero.

I numerically solved equations (2.12-2.16, 2.23-2.24) using the fourth order Runge-Kutta method, for cable length $L = 0.5$ and injected current ramp

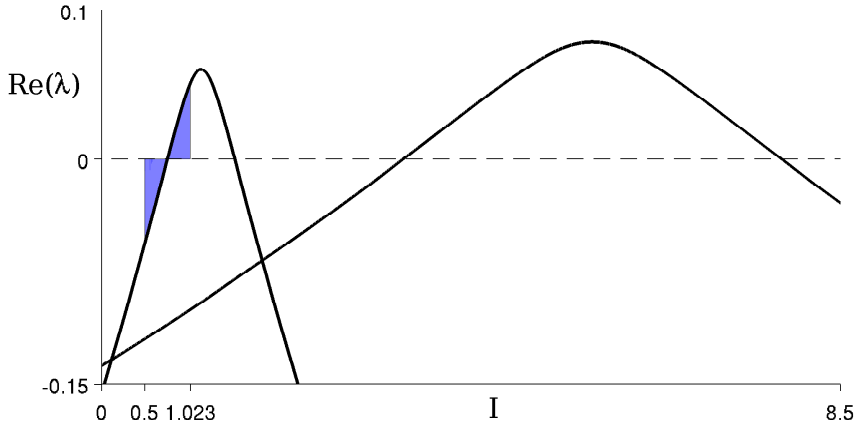

Figure 2: $G_{ss1} = 0.05$, $G_{ss2} = 0.01$. WKB prediction for I_j in response to the slow linear current ramp $I(t) = 0.5 + \epsilon t$.

$I(t) = 0.5 + \epsilon t$; trials were done for a large number of small ramp speeds ϵ. Figure 3 shows the results of these numerical solutions. The top panel is a plot of the apparent firing threshold I_j observed in a trial, defined as the value of injected current at the time the potential in one of the two spines exceeds 0.5, versus the inverse of the ramp speed used in that trial. As one moves to the right across the graph, the ramp speed $\epsilon \to 0$ and one enters the regime in which the WKB prediction is valid. The bottom panel plots the potentials in the two spines as a function of time (spine one in black, spine two in red), for the specific choice of ramp speed $\epsilon = 0.001$.

One sees that there is good agreement between the WKB prediction of $I_j = 1.023$ and the numerical solution of the ordinary differential equation. The "jitter" pattern that is observed is characteristic of this plot and is discussed in [22]. I note that the large oscillations in membrane potential which commence at I_j are found only in spine one.

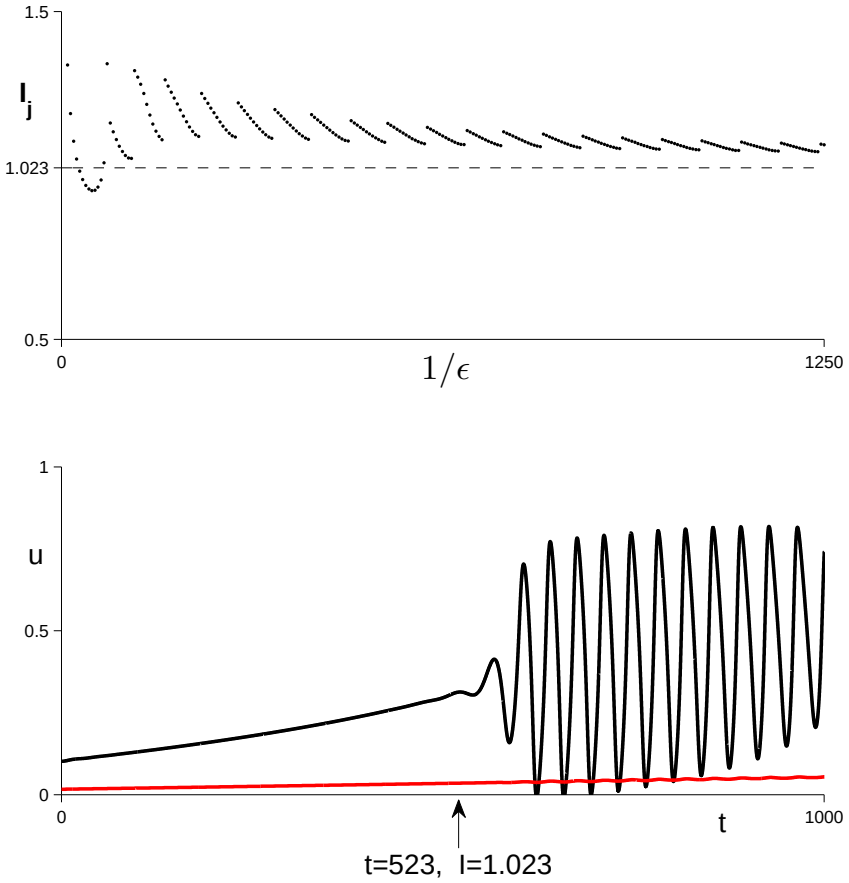

Figure 3: $G_{ss1} = 0.05$, $G_{ss2} = 0.01$. $I(t) = 0.5 + \epsilon t$. *Top*: I_j obtained from numerical solutions. *Bottom*: Time course of spinehead potentials for the ramp speed $\epsilon = 0.001$.

I now switch the stem conductances, and consider $G_{ss1} = 0.01$, $G_{ss2} = 0.05$. Figure 4 shows the plot of $Re(\lambda)$ versus I; one sees that it is very similar to Figure 1. Figure 5 shows the WKB prediction for I_j in response to the same slow current ramp $I = 0.5 + \epsilon t$. The system is predicted to go unstable at $I_j = 1.233$, very similar to the prediction for the case $G_{ss1} = 0.05$, $G_{ss2} = 0.01$.

Figure 6 shows that numerical solutions yielded good agreement with this prediction. The graph of the time course of potentials in the two spines shows

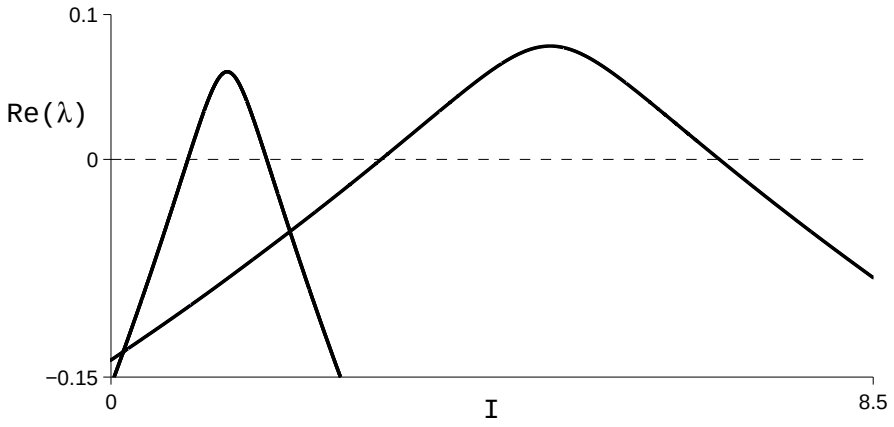

Figure 4: $G_{ss1} = 0.01$, $G_{ss2} = 0.05$. $Re(\lambda(I))$ versus I for the four eigenvalues associated with the system.

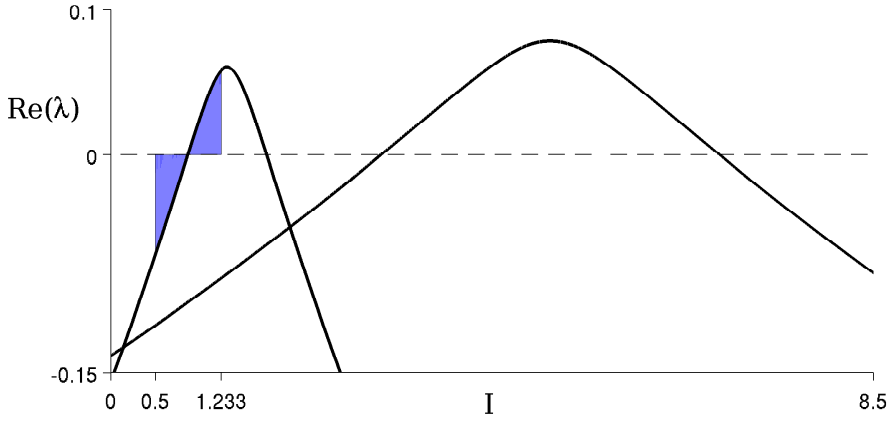

Figure 5: $G_{ss1} = 0.01$, $G_{ss2} = 0.05$. WKB prediction for I_j in response to the slow linear current ramp $I(t) = 0.5 + \epsilon t$.

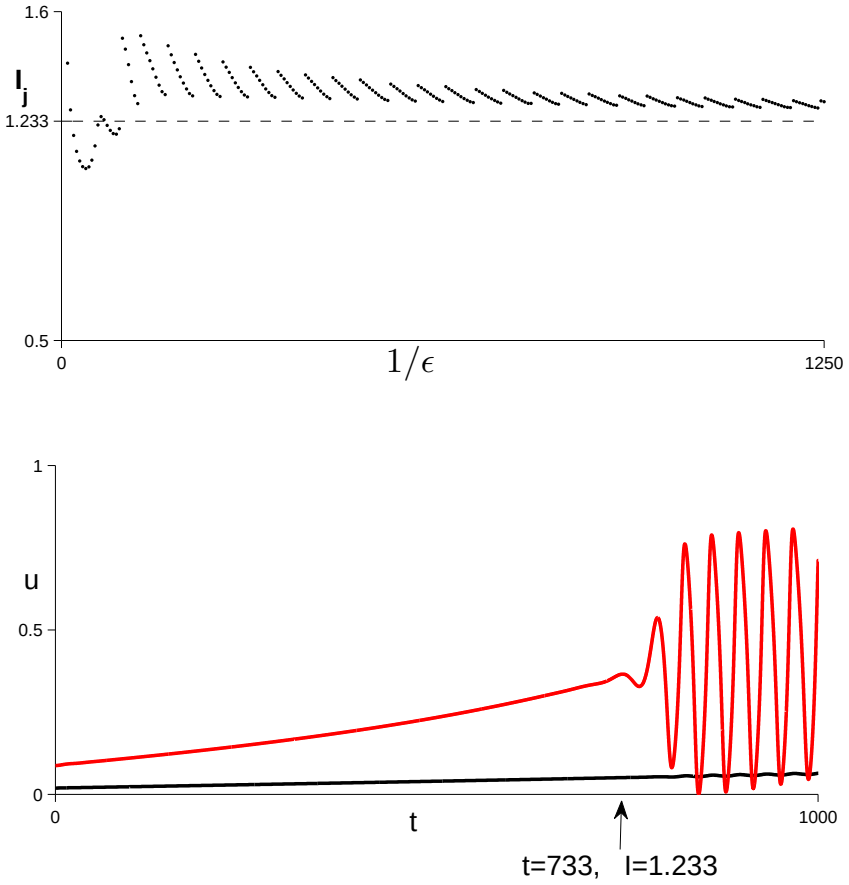

Figure 6: $G_{ss1} = 0.01$, $G_{ss2} = 0.05$. $I(t) = 0.5 + \epsilon t$. *Top*: I_j determined from numerical solutions. *Bottom*: Time course of spinehead potentials for the ramp speed $\epsilon = 0.001$.

the one major difference between this case and that of $G_{ss1} = 0.05$, $G_{ss2} = 0.01$: now, the large-amplitude oscillations arise in spine two, at the end of the cable opposite the site of current injection.

These two cases indicate that with a spatially extended excitable system it is possible that the instability will not arise uniformly throughout the system once I attains I_j. In the next section I show that a closer analysis of information obtained from the WKB method indicates where the instability will

arise.

WKB prediction for location at which oscillations arise

Consider the 4-dimensional u_1, w_1, u_2, w_2 phase-space in which solution trajectories evolve when one injects the cable with a slow current ramp. A given solution trajectory is attracted to the slowly-varying solution at $t = 0$, and remains close to it until the apparent firing threshold I_j is attained. Once this occurs, the trajectory shoots away from the slowly-varying solution in a direction in phase space dictated by $\vec{v_j}$, where $\vec{v_j}$ is the eigenvector associated with the eigenvalue responsible for the onset condition being satisfied, evaluated at $I = I_j$. This suggests that by inspecting $\vec{v_j}$ one can determine where the instability will arise. To be precise, I note that the onset condition is satisfied by a complex conjugate pair of eigenvalues, associated with a complex conjugate pair of eigenvectors. Figure 7 shows one of the $\vec{v_j}$ for the cases $G_{ss1} = 0.05$, $G_{ss2} = 0.01$ (top) and $G_{ss1} = 0.01$, $G_{ss2} = 0.05$ (bottom).

For the case $G_{ss1} = 0.05$, $G_{ss2} = 0.01$, the components of $\vec{v_j}$ are such that the initial movement away from the slowly-varying solution once I attains I_j are nearly confined to the $u_1 w_1$ plane in phase space, associated with the first spine. For the case $G_{ss1} = 0.01$, $G_{ss2} = 0.05$, the components $\vec{v_j}$ are such that the initial movement away from the slowly-varying solution are nearly confined to the $u_2 w_2$ plane, corresponding to spine two.

Returning to the case $G_{ss1} = 0.05$, $G_{ss2} = 0.01$ I note that the second spine does eventually fire, but for a much larger value of current as indicated by Figure 8. One may predict the current value at which spine two fires by another application of the WKB method. I note that while spine one is firing, which goes on for a bit even after the second Hopf point is reached, the state

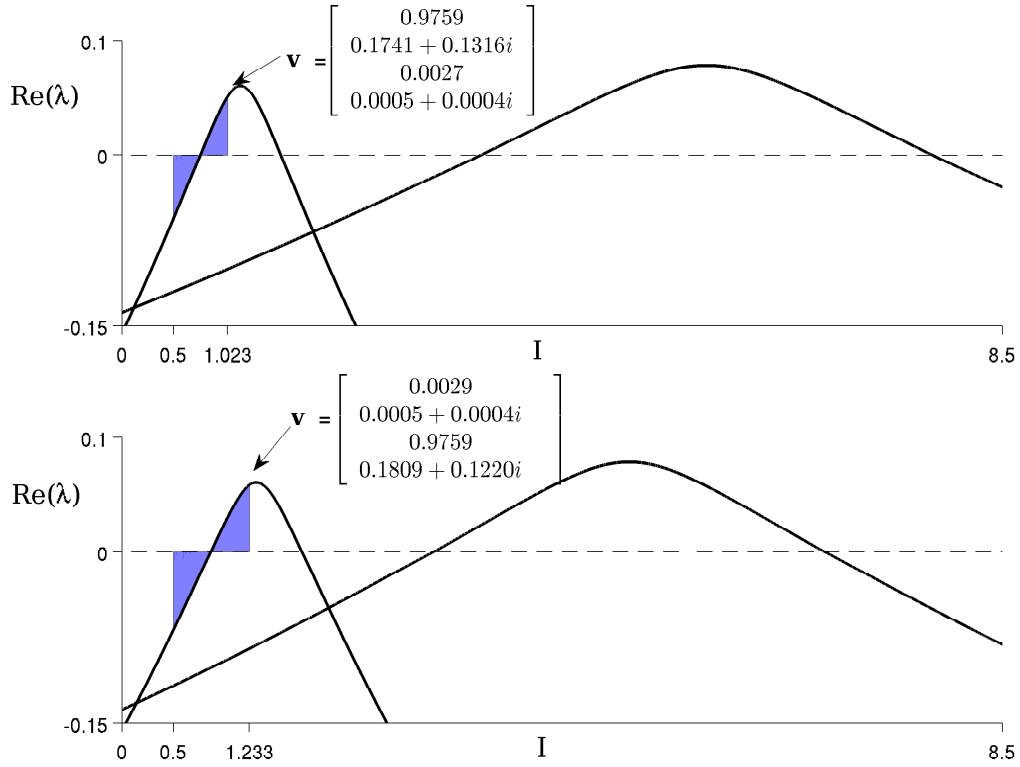

Figure 7: *Top*: WKB prediction for I_j in response to the slow linear ramp $I(t) = 0.5 + \epsilon t$. $G_{ss1} = 0.05$, $G_{ss2} = 0.01$. *Bottom*: Same, for the case $G_{ss1} = 0.01$, $G_{ss2} = 0.05$.

of the system is not near enough to the slowly-varying solution for the linear WKB analysis to be valid. However, near $I = 1.75$ the system has settled down once more. At this point, one may view the problem as being restarted, this time with the slow current ramp $I = 1.75 + \epsilon t$. Another application of the WKB method indicates that the system will again become unstable at $I_j = 5.171$. This time, the other complex conjugate pair of eigenvalues is responsible for satisfying the onset condition. An inspection of one of the eigenvectors associated with it indicates that now the instability arises in spine two. This is confirmed in Figure 8.

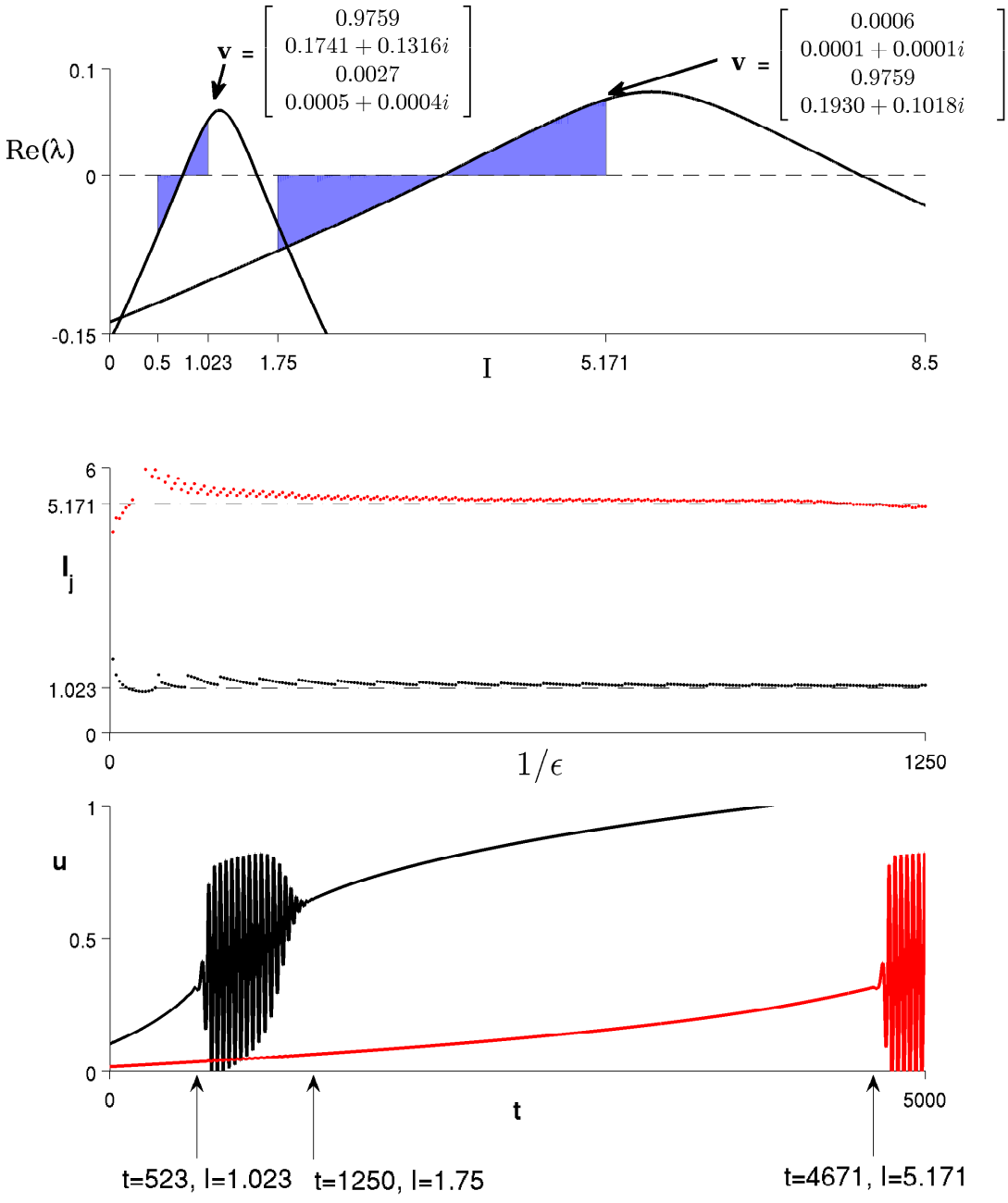

Figure 8: $G_{ss1} = 0.05$, $G_{ss2} = 0.01$. $I(t) = 0.5 + \epsilon t$. *Top*: WKB prediction for I_j. *Middle*: I_j determined from numerical solutions. *Bottom*: Time course of spinehead potentials for the ramp speed $\epsilon = 0.001$.

I note that for the cases of stem conductance so far considered, the functional dependence of the eigenvalues on I is such that there are four crossings of the imaginary axis as I increases from zero: one complex conjugate pair is responsible for the first two crossings, and another is responsible for the second two crossings. Furthermore, inspection of the eigenvectors for all I in the range considered (not shown) indicates that the eigenvalue responsible for the first two crossings of the imaginary axis is associated almost exclusively with the spine having stem conductance $G_{ss} = 0.05$, and the eigenvalue responsible for the second two crossings is associated almost exclusively with the spine having the lower stem conductance $G_{ss} = 0.01$. This indicates that for these conductances and a cable of electrotonic length $L = 0.5$, the two spines behave relatively independently of each other. In the next section I investigate the extent to which this continues to hold as the stem conductances are varied.

2.3 Effect of varying stem conductances

In Figure 9 I fix the stem conductance of the first spine at $G_{ss1} = 0.01$ and plot the values of I satisfying $Re(\lambda(I)) = 0$ as G_{ss2} varies.

For each value of G_{ss2}, the situation is as described in the previous section: the two spines behave relatively independently, each being associated with a single complex conjugate pair of eigenvalues as indicated by inspecting the eigenvectors. The two curves which are increasing with I and are nearly straight are associated with spine one; as G_{ss2} increases, more current is diverted into spine two for a given value of I, which causes an increase in the Hopf points associated with spine one. For the same reason, the Hopf points associated with spine two decrease as G_{ss2} increases (the two curved lines). I note that the Hopf points associated with spine two eventually coalesce and

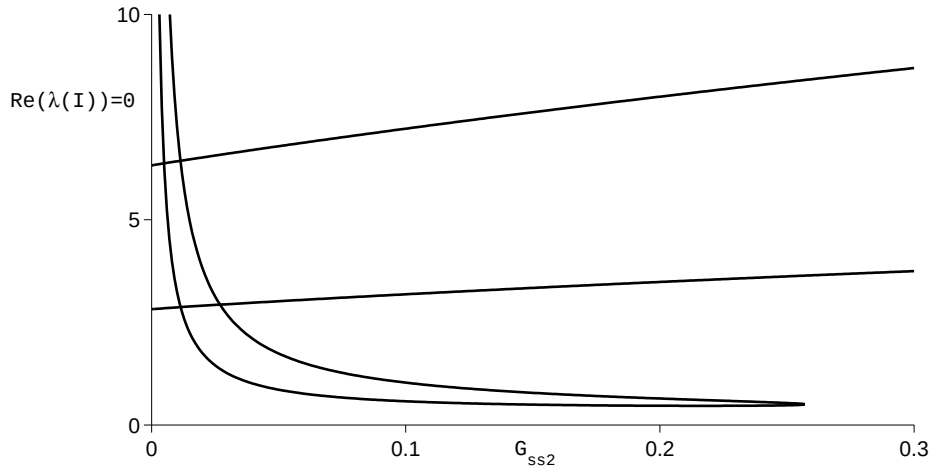

Figure 9: Values of I satisfying $Re(\lambda(I)) = 0$; G_{ss1} is held fixed at 0.01 while G_{ss2} is allowed to vary. The two spines remain relatively independent, each possessing its own two Hopf points.

disappear; at this point the conductance load due to the passive cable precludes the onset of oscillations in spine two for any value of injected current; cf. Fig. 3-4 in Wu and Baer [30]. It is not surprising that the two spines behave relatively independently even for large values of G_{ss2}, as spine one has a low value of stem conductance. Contrast this with Figure 10, in which I hold the stem conductance of spine one fixed at the much larger value of $G_{ss1} = 0.2$.

A casual inspection of Figure 10 suggests that for large values of G_{ss2}, the spines no longer behave independently. As G_{ss2} increases, the upper Hopf point of spine one and the lower Hopf point of spine two coalesce and disappear, and one is left with two Hopf points of a single excitable system. To investigate further, I examined the case $G_{ss1} = 0.2$, $G_{ss2} = 0.2$. Figure 11 shows a plot of $Re(\lambda)$ versus I.

The system now has only a single complex conjugate pair of eigenvalues which attain positive real part as I increases. Figure 12 shows the WKB

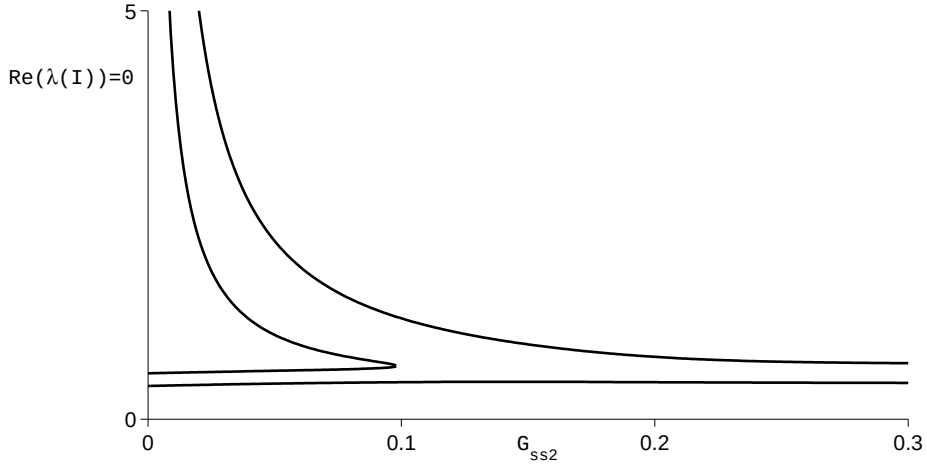

Figure 10: Values of I satisfying $Re(\lambda(I)) = 0$; G_{ss1} is held fixed at 0.2 while G_{ss2} is allowed to vary.

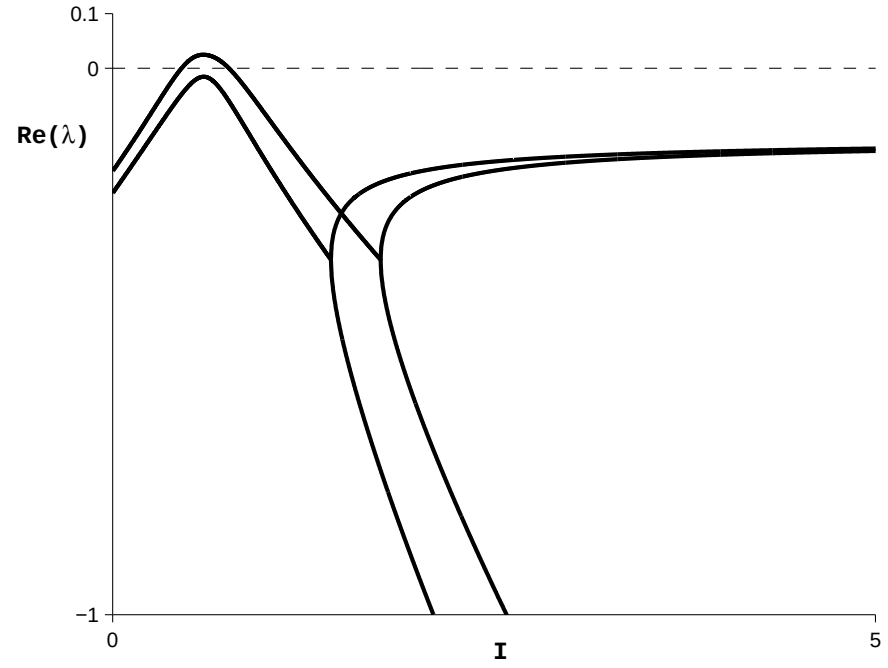

Figure 11: $G_{ss1} = G_{ss2} = 0.2$. $Re(\lambda(I))$ versus I. The system has two Hopf points for these choices of stem conductance.

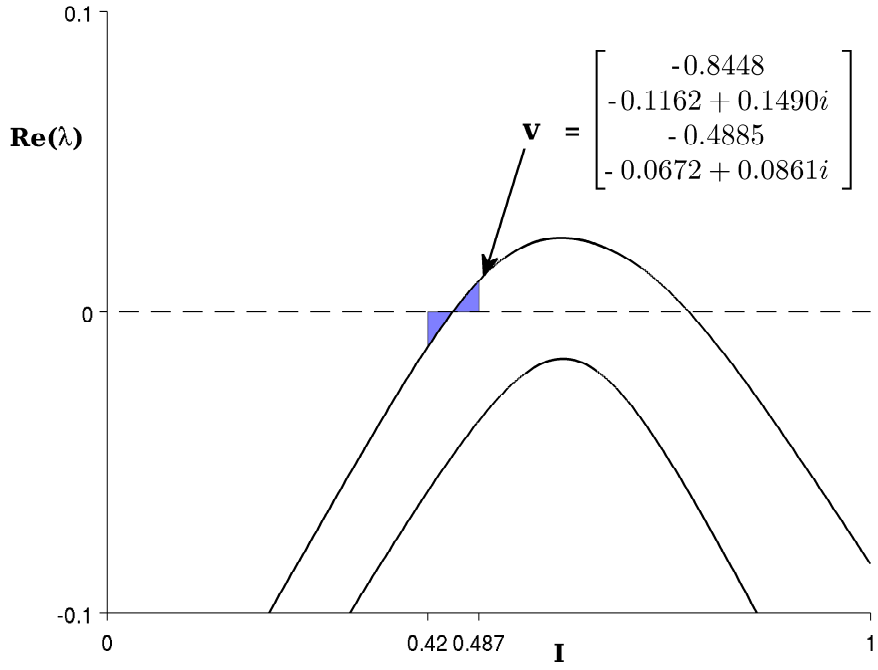

Figure 12: $G_{ss1} = G_{ss2} = 0.2$. WKB prediction for the apparent firing threshold I_j and the location at which oscillations arise in response to the slow linear current ramp $I(t) = 0.42 + \epsilon t$.

prediction for the firing threshold and location at which oscillations arise in response to the slow current ramp $I = 0.42 + \epsilon t$. Oscillations are expected to arise in both spines, but with a slightly larger amplitude in spine one. Figure 13 shows the results of numerical solutions.

The graph of apparent firing threshold versus inverse ramp speed suggests that the actual value of the firing threshold slightly exceeds the WKB prediction of $I_j = 0.487$. This is due to the fact that $Re(\lambda)$ at $I_j = 0.487$ is very small, and the exact onset condition (see Appendix) for $O(1)$ deviation from the slowly-varying solution is

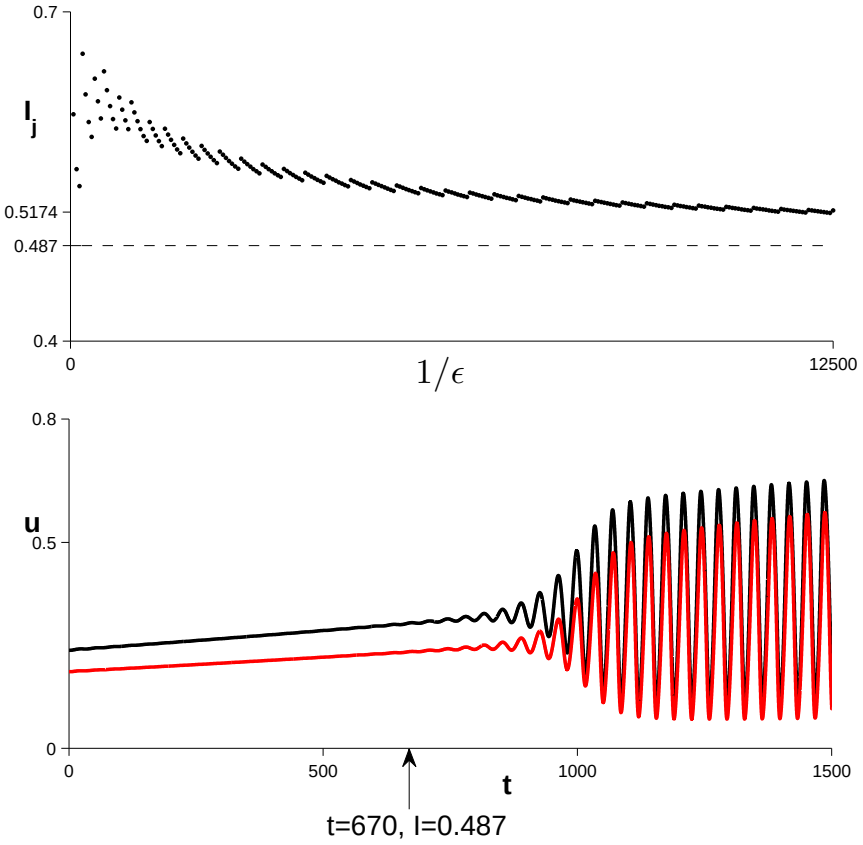

Figure 13: $G_{ss1} = G_{ss2} = 0.2$. $I(t) = 0.42 + \epsilon t$. *Top*: I_j obtained from numerical solutions. *Bottom*: Time course of potential in the two spineheads for the particular ramp speed $\epsilon = 0.0001$.

$$\int_{I_0}^{I_j} Re(\lambda(I))dI = O(\epsilon). \tag{2.25}$$

The initial condition was chosen to be near the slowly-varying solution at $I_0 = 0.42$, and the time course indicates that the predicted value of $I_j = 0.487$ is where visible deviation from the slowly-varying solution begins. Compare this with the results for the ramp $I = 0.3 + \epsilon t$: again, the WKB method predicts that oscillations will arise in both spines (Fig. 14), but this time

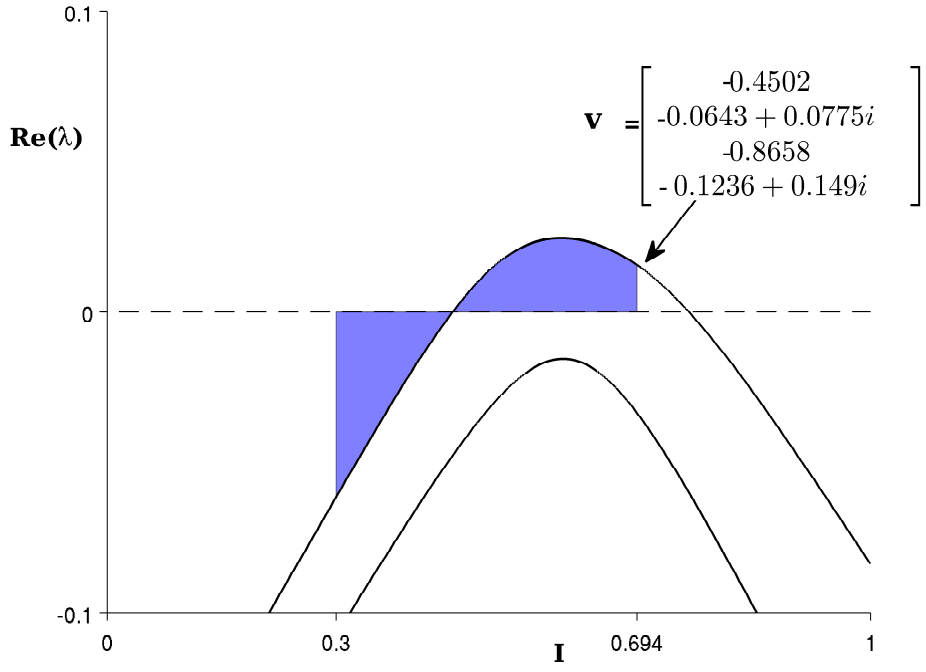

Figure 14: $G_{ss1} = G_{ss2} = 0.2$. WKB prediction for the apparent firing threshold I_j and the location at which oscillations will arise in response to the slow linear current ramp $I(t) = 0.3 + \epsilon t$.

the amplitude of the oscillations away from the slowly-varying solution are predicted to be slightly larger in spine two. This is confirmed in Figure 15.

2.4 Discussion

I have investigated a simple system with spatial extension, in which two active spines are coupled diffusively through a passive cable of electrotonic length $L = 0.5$. I confirmed the memory effect for slow current ramps, in which choosing a smaller value of initial current results in a higher apparent firing threshold. Interestingly, I found that the onset of sustained oscillations might arise in the spine located at the cable end opposite the site of current injection. I found that the WKB analysis from which one determines the apparent firing

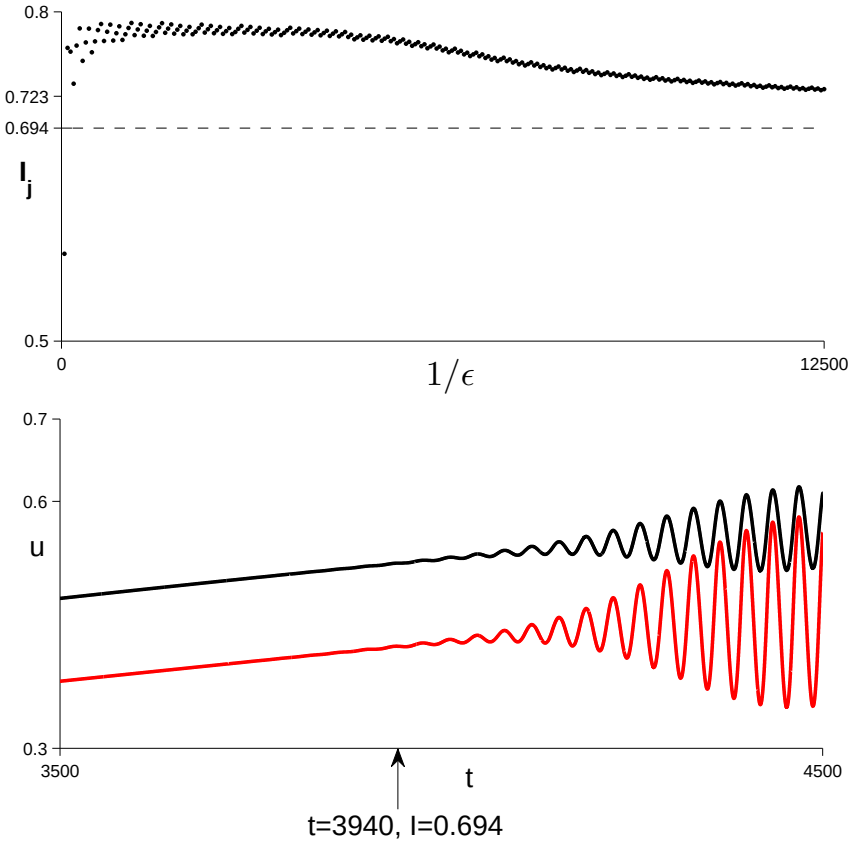

Figure 15: $G_{ss1} = G_{ss2} = 0.2$. $I(t) = 0.3 + \epsilon t$. *Top*: I_j obtained from numerical solutions. *Bottom*: Time course of potential in the two spineheads for the particular ramp speed $\epsilon = 0.0001$.

threshold also provides information on where oscillations will arise. This is obtained by inspecting the eigenvector associated with the eigenvalue satisfying the onset condition.

When the stem conductances are low ($G_{ss1} = 0.01$, $G_{ss2} = 0.05$ and $G_{ss1} = 0.05$, $G_{ss2} = 0.01$), the spines behave relatively independently of each other, retaining individual Hopf points. When stem conductances are higher ($G_{ss1} = G_{ss2} = 0.2$), the spines are heavily coupled, and the system has two

Hopf points. Destabilization then occurs in both spines, but the amplitude of oscillations away from the slowly-varying solution is slightly larger for spine one if I_j occurs near the system's first Hopf point, and slightly larger for spine two if I_j occurs near the system's second Hopf point. This corresponds to a change in the components of $\vec{v_j}$, the eigenvector associated with the eigenvalue satisfying the onset condition, evaluated at I_j.

The distal initiation of firing for the case of low stem conductances occurs when spine two has the higher stem conductance and hence experiences a stem current in its firing range before spine one does. In the next chapter I show a more interesting example of distal initiation of firing, for a spiny cable in which all stem conductances are identical. As will be shown, this is a more dramatic version of the same phenomenon observed for the case $G_{ss1} = G_{ss2} = 0.2$, in which spine two experiences slightly larger-amplitude oscillations away from the slowly-varying solution than does spine one when I_j significantly exceeds the first Hopf point.

Chapter 3

RESPONSE OF THE FITZHUGH-NAGUMO SPINY CABLE TO A SLOW CURRENT RAMP

3.1 Continuum model of the FitzHugh-Nagumo spiny cable

I investigated a continuum model of a passive dendritic shaft studded with excitable dendritic spines. This model, which is due to Baer and Rinzel [3], treats the spines as being continuously distributed along the length of the shaft as dictated by the continuous density function $\bar{n}(x)$. This results in a model which can be succinctly mathematically stated, even when one is dealing with a large number of spines; this is in contrast to models which handle each spine via boundary conditions (as in the last chapter), or as a distinct compartment. I emphasize that although the spines are modeled as a continuum, the model is such that the spines only interact indirectly via the dendritic shaft.

Baer and Rinzel modeled a dendritic shaft with passive cable properties. Current flows in an axial direction in response to a potential gradient along the shaft, and a leakage current flows in a direction transverse to the membrane. The passive shaft is coupled to excitable spines, which contain voltage-gated ion channels enabling them to undergo action potentials in response to a current impulse. The degree of coupling between the dendritic shaft and the spines is determined by the spine stem conductance G_{ss}; the cable properties of the spine stems are neglected and the stem is modeled as a lumped Ohmic resistance. Baer and Rinzel modeled the spines as obeying Hodgkin-Huxley dynamics [3]. Several authors have investigated Baer-Rinzel continuum models in which other dynamics are chosen for the spines; for example, Zhou [32] and Chen and Bell [5] studied the model for spines obeying Nagumo dynamics

(FitzHugh-Nagumo without the slow recovery variable). Here I have chosen to investigate FitzHugh-Nagumo dynamics.

Under the continuum approximation, at time t a cable segment of tiny length Δx centered at point x along the shaft receives current $\bar{n}(x)\Delta x I_{ss}(x,t)$ from the spines. I_{ss} is the current flowing into the shaft from a single spine through its stem, due to the difference in potential between that spine and the shaft, and is given by $I_{ss}(x,t) = G_{ss}(u(x,t) - V(x,t))$, where u denotes potential in the spines and V denotes the potential in the shaft. Let X be electrotonic length, that is, length measured in units of the cable length constant $\lambda = \sqrt{\frac{R_m d}{4R_i}}$. Then the Baer-Rinzel continuum model for the FitzHugh-Nagumo spiny cable can be written as

$$\tau \frac{\partial V}{\partial t} = \frac{\partial^2 V}{\partial X^2} - V + \bar{n}(X) R_\infty I_{ss}(X) \tag{3.1}$$

$$\frac{\partial u}{\partial t} = -f(u) - w - I_{ss}(X) \tag{3.2}$$

$$\frac{\partial w}{\partial t} = b(u - \gamma w) \tag{3.3}$$

where τ is the dendritic membrane time constant, $\bar{n}(X)$ is the spine density (number of spines per electrotonic length), and $R_\infty = R_m/\pi\lambda d$. For uniform distributions of spines along the shaft, the continuum model is a good approximation provided that the spine density is sufficiently large [3].

I considered the case of a spiny FitzHugh-Nagumo cable of dimensionless length L with current $I = I_0 + g(\epsilon t)$ injected into one end and the other end sealed to current. This gives rise to the boundary conditions:

$$\frac{\partial V}{\partial X}(0,t) = -R_\infty I(t) \tag{3.4}$$

$$\frac{\partial V}{\partial X}(L,t) = 0. \tag{3.5}$$

3.2 Methods

I note that this system is a partial differential equation (PDE) and the WKB analysis being used applies to ordinary differential equations (ODE). However, using a compartmental approach one can approximate the PDE as a system of first-order differential equations. Let the first compartment ($i = 1$) correspond to the end at which current is injected. The equations governing compartment i where $2 \leq i \leq n-1$ are

$$\dot{u_i} = -f(u_i) - w_i - G_{ss}(u_i - V_i) \tag{3.6}$$

$$\dot{w_i} = b(u_i - \gamma w_i) \tag{3.7}$$

$$\tau \dot{V_i} = -V_i + \frac{(V_{i+1} - 2V_i + V_{i-1})}{\Delta X^2} + \bar{n} R_\infty G_{ss}(u_i - V_i) \tag{3.8}$$

where ΔX is the length of one compartment.

The boundary conditions were handled as follows. A finite difference scheme for solving the PDE would break the length of the cable up into n equally spaced grid points x_1 through x_n. The compartments correspond to the grid points in the following way: compartment i is centered on grid point i. The finite difference scheme would handle the boundary condition for the external current by introducing a "ghost point" labeled x_0. At each time step, x_0 would be assigned the value V_0 that makes the following equation true:

$$V_0 - V_2 = 2RI \tag{3.9}$$

where $R = R_\infty \Delta X$ is the resistance associated with one compartment. In this spirit, I introduced a "ghost compartment" that acts as a second neighbor to compartment one, having voltage

$$V_0 = V_2 + 2R_\infty \Delta X I. \tag{3.10}$$

Similarly, a ghost compartment was introduced at the far end of the cable, with voltage

$$V_{n+1} = V_{n-1}. \tag{3.11}$$

The equations governing the first and last compartments are as given in (3.6-3.8) with V_0 and V_{n+1} defined as above.

The compartmental model with n compartments is a $3n-$dimensional ODE of general form

$$\dot{\vec{x}} = f(\vec{x}, I(\epsilon t)) \tag{3.12}$$

and for convenience when analyzing eigenvector components, I chose to arrange the equations such that for the $i'th$ compartment,

$$\dot{u_i} = x_i \tag{3.13}$$

$$\dot{w_i} = x_{i+n} \tag{3.14}$$

$$\tau \dot{V_i} = x_{i+2n}. \tag{3.15}$$

The WKB procedure requires that for each I in some range, one computes the steady state $\overrightarrow{x}_{ss}(I)$, the Jacobian of the system evaluated at this steady state, the eigenvalues of the Jacobian, and the integral for the onset condition

$$\int_{I_0}^{I} [g^{-1}(I - I_0)]' Re(\lambda(I)) dI$$

for each eigenvalue of the Jacobian. A MATLAB program was written to carry out these steps. The program uses fsolve to determine the steady state for each I, the DERIVEST suite of functions to compute the Jacobian via numerical differentiation, and the function eig to determine the eigenvalues and associated eigenvectors. A program was also written to keep track of the separate eigenvalue integrals, and determine the value of I, denoted by I_j, at which one of these integrals becomes positive. This I_j is the WKB prediction for the value of injected current at the onset of sustained oscillations in the spinehead potential. The eigenvector $\vec{v}_j$ corresponding to this critical eigenvalue, evaluated at I_j (notice that the eigenvectors are also functions of I), provides a prediction of where along the cable the instability will first show itself.

WKB prediction for I_j

I illustrate my technique for a cable of dimensionless length $L = 3$, studded with 75 uniformly distributed FitzHugh-Nagumo spines, with uniform spine stem conductances $G_{ss} = 0.1$. I used 75 compartments, corresponding to the 225-dimensional system

$$\dot{x_i} = -f(x_i) - x_{i+75} - G_{ss}(x_1 - x_{i+150}), \qquad 1 \le i \le 75 \quad (3.16)$$

$$\dot{x_i} = b(x_{i-75} - \gamma x_i), \qquad 76 \le i \le 150 \quad (3.17)$$

$$\dot{x_{151}} = -x_{151} + \frac{(x_{152} - 2x_{151} + V_0)}{\Delta X^2} + \bar{n} R_\infty G_{ss}(x_1 - x_{151}) \quad (3.18)$$

$$\dot{x_i} = -x_i + \frac{(x_{i+1} - 2x_i + x_{i-1})}{\Delta X^2} + \bar{n} R_\infty G_{ss}(x_{i-150} - x_i), \; 152 \le i \le 224 \quad (3.19)$$

$$\dot{x_{225}} = -x_{225} + \frac{(x_{224} - 2x_{225} + V_{76}}{\Delta X^2} + \bar{n} R_\infty G_{ss}(x_{75} - x_{225}). \quad (3.20)$$

In the above system, $\Delta X = 0.04$, $\bar{n} = 25$, $R_\infty \approx 0.31831$, and equations (3.4-3.5) dictate that V_0 and V_{76} be defined as

$$V_0 = x_{152} + 2R_\infty \Delta X I \quad (3.21)$$

$$V_{76} = x_{224}. \quad (3.22)$$

All FitzHugh-Nagumo spines are identical, with parameters $a = 0.14$, $b = 0.05$, and $\gamma = 2.54$.

My program generated the 225 functions $\lambda_i(I)$, $1 \le i \le 225$. Fig. 16 shows the plot of the real portion of the eigenvalue satisfying the onset condition (actually, a complex conjugate pair) versus I. The real portion of the eigenvalue is responsible for the onset of instability under the WKB prediction.

A note on the number of compartments used: too few compartments will lead to error as the compartments must be small enough that the three variables u, w, and V are approximately constant over the length of the compartment. To ensure that 75 was a sufficient number of compartments, I performed the same computations as above for the case in which the cable was broken

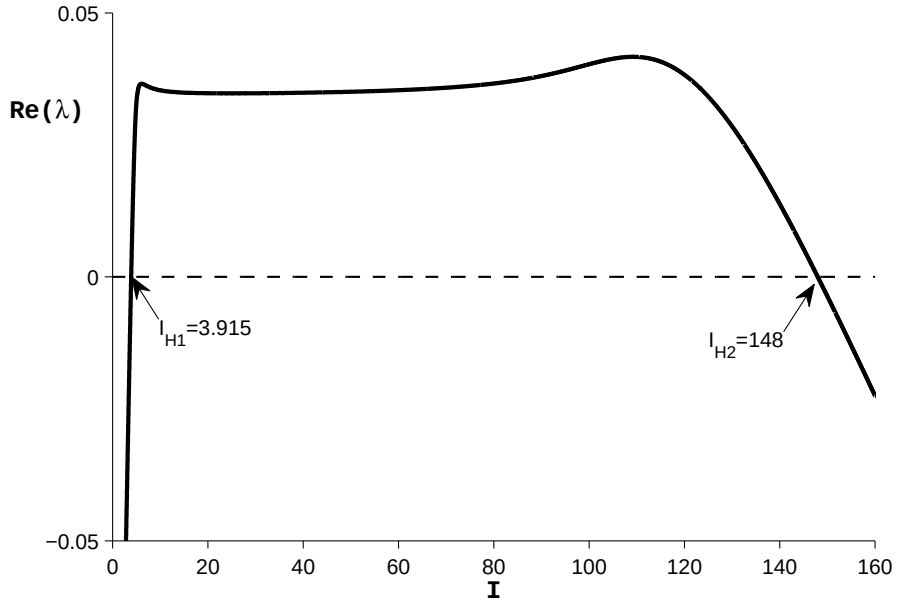

Figure 16: $Re(\lambda(I))$ for the eigenvalue responsible for the onset of instability under the WKB prediction. 75 uniformly distributed spines on a passive cable of length $L = 3$. $G_{ss} = 0.1$ for all spines.

into 100 compartments; this resulted in 300 functions $\lambda(I)$, one of which is responsible for the onset of instability. I found that there was near-perfect overlap of this $\lambda(I)$ with that shown in Fig. 16, obtained with 75 compartments. Hence, 75 was a large enough number of compartments to use. It is computationally efficient to use only as many compartments as needed.

I considered the response of the spiny cable to a slow linear current ramp given by $I(t) = 1.25 + \epsilon t$, $\epsilon \to 0$. The WKB prediction for I_j satisfies

$$\int_{1.25}^{I_j} Re(\lambda) dI = 0. \tag{3.23}$$

Figure 17 indicates the region of $Re(\lambda)$ that was integrated and the resulting prediction for I_j.

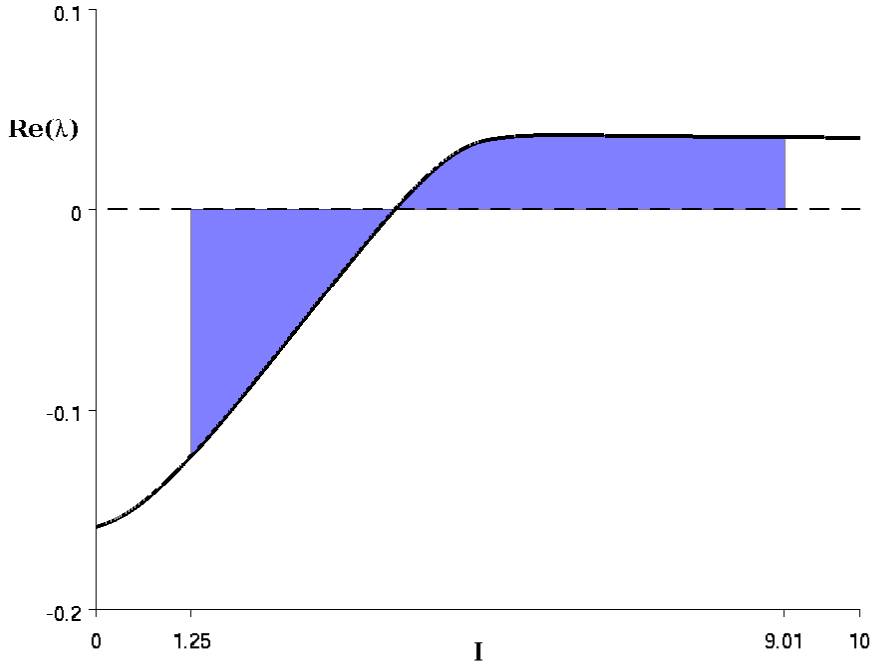

Figure 17: WKB prediction for I_j in response to the slow current ramp $I(t) = 1.25 + \epsilon t$, $\epsilon \to 0$.

The WKB method predicts that the spiny cable will go unstable when the injected current ramps reaches $I \approx 9.01$. This prediction was compared with numerical solutions of equations (3.1-3.5) obtained using the semi-implicit finite difference method used in [29], for a large number of ramp speeds ϵ. Fig. 18 plots I_j as observed in numerical solutions versus the inverse ramp speed $1/\epsilon$. As one moves to the right along the x-axis, the ramp speed $\epsilon \to 0$ and one enters the regime of applicability of the WKB prediction. One can see that the observed I_j asymptotically approaches the WKB prediction of $I_j = 9.01$ before coming back down again in a way that is indicative of round-off error [1]; a major difficulty with implementing very slow current ramps is the very large number of time steps they require; this leads to round-off

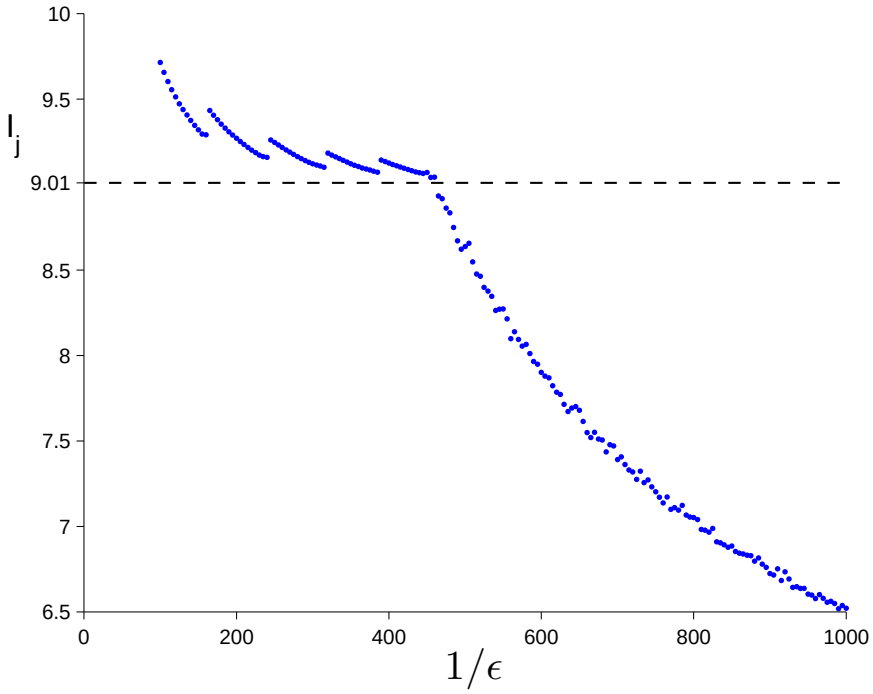

Figure 18: I_j obtained from numerical solutions of the FitzHugh-Nagumo spiny cable's response to the slow current ramp $I = 1.25 + \epsilon t$.

error, which causes numerical solutions to destabilize earlier than they would if infinite precision were available. All numerical solutions in this thesis were computed in quadruple precision arithmetic.

WKB prediction for the location at which oscillations arise.

The second part of the WKB prediction is *where* the onset of oscillations will occur along the cable. To predict this, I inspected the eigenvector associated with the eigenvalue causing instability, evaluated at $I_j = 9.01$. This eigenvector, which I call $\vec{v}_j$, has 225 components. Components 1-75 correspond to spinehead potential variables u_1 through u_{75}, components 76-150 correspond to slow recovery variables w_1 through w_{75}, and components 151-225 correspond to dendritic shaft potential variables V_1 through V_{75}. I performed the

following procedure on $\vec{v}_j$: (1) Compute the modulus of each component, $|v_i|$ (note that in general the components are complex numbers). (2) Divide each of these moduli by $|v_1|$, the modulus of the first component, so that I obtain a vector of relative moduli $\frac{|v_i|}{|v_1|}$; this makes the third step easier. (3) Plot these relative moduli against the vector index, and note whether one of these stands out as being much larger than all others. If so, the variable corresponding to that component will undergo the largest-amplitude oscillations away from the slowly-varying solution once the system loses stability, and the compartment (equivalently, the location along the cable) associated with that variable will be where the instability arises.

In practice, the component with largest modulus of $\vec{v}_j$ always occurs in indices 1-75; that is, the instability first shows itself in the spinehead potentials. In Fig. 19 I show the plot used to predict the location at which oscillations will begin. One finds that the twelfth component of $\vec{v}_j$ has the largest modulus; it exceeds the modulus of the first component by a factor of more than 60. The twelfth component of $\vec{v}_j$ corresponds to the potential in the spine located at compartment 12. Since the cable is of length $L = 3$, this corresponds to a location $x \approx 0.48$. Hence, I predicted that when the cable enters into sustained oscillations at $I_j = 9.01$, the instability would first become apparent at a distance of about 0.5 from the injection point.

I checked this WKB prediction against finite difference solutions of equations (3.1-3.5), using ramp speed $\epsilon = 0.004$. From Fig. 18 one sees that this ramp speed is small enough for the WKB method to be applicable, and not so small that roundoff error is a problem. Hence, the injected current obeys $I = 1.25 + 0.004t$. Fig. 20 provides spatial profiles of the potential in the spineheads versus distance x along the cable, at a few instants of time near

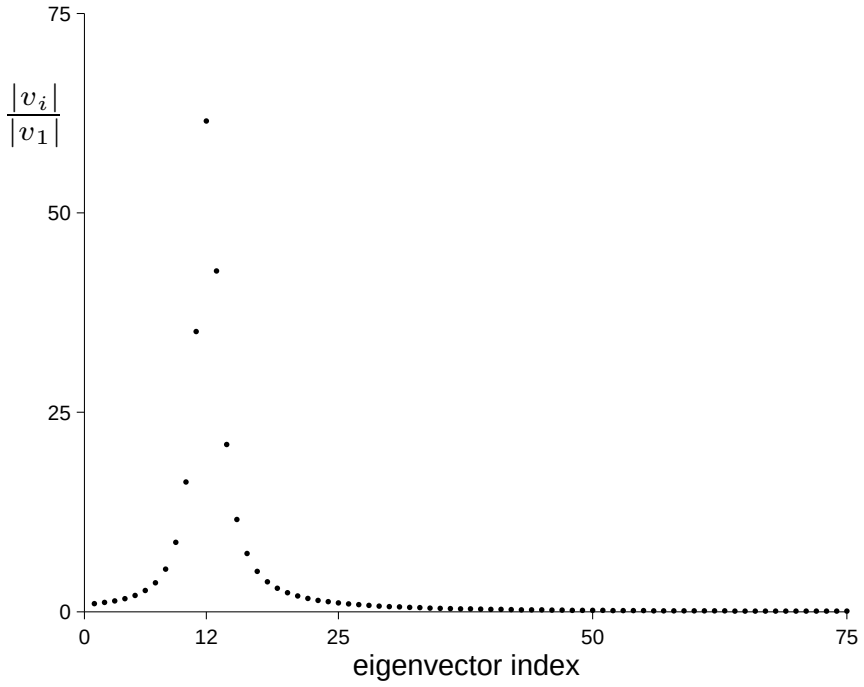

Figure 19: WKB prediction for the location along the FitzHugh-Nagumo spiny cable at which oscillations arise.

the onset of instability. One sees that the finite difference solutions confirm the WKB prediction of $x \approx 0.48$ for the location at which oscillations first become apparent.

3.3 Results

I investigated the response of a spiny FitzHugh-Nagumo cable of length $L = 3$ to various slow current ramps, and compared numerical solutions with the WKB predictions for I_j and for the cable location at which oscillations ensue once I_j is attained. All cable parameters are as given as in section 3.2 except where otherwise noted. I found three types of spiny cable response, depending on the degree of electrical coupling between the excitable spines and the passive cable as determined by the spine stem conductance G_{ss}.

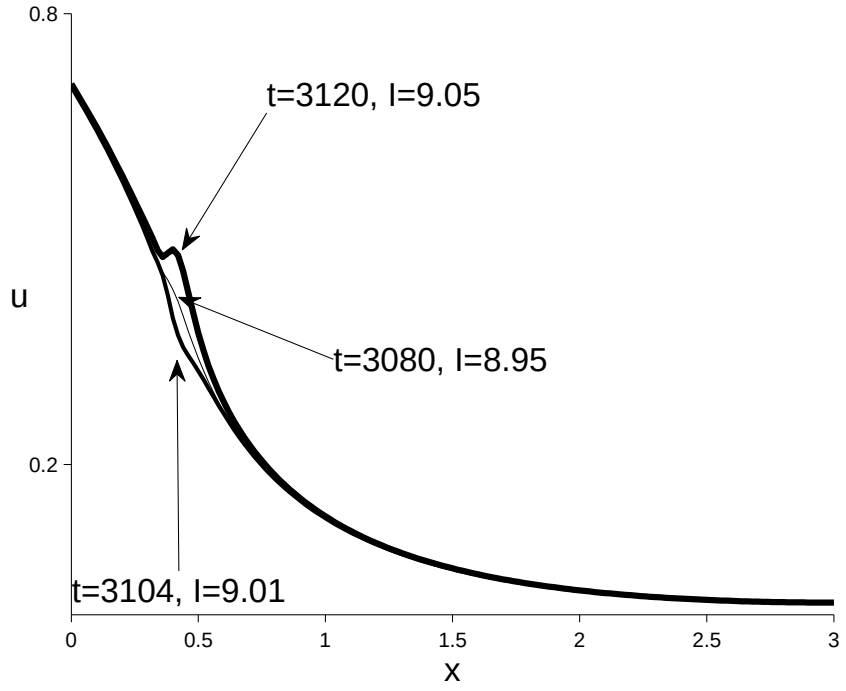

Figure 20: Spatial profiles of the potential in the spineheads at a few instants of time near the onset of instability, obtained from numerical solutions.

Low spine stem conductance

I considered the case of 75 uniformly distributed spines ($\bar{n} = 25$), each with spine stem conductance $G_{ss} = 0.02$. 75 compartments were used to perform the WKB analysis. Of the resulting 225 eigenvalues, 150 (75 complex-conjugate pairs) have nonzero imaginary part for I in the range considered. Fig. 21 shows a plot of their real parts. All other eigenvalues are large and negative.

I investigated the spiny cable response to the slow current ramp $I(t) = 3 + \epsilon t$, $\epsilon \to 0$. According to the WKB method, the eigenvalue responsible for the first Hopf point is the one responsible for the onset of instability in response to this current ramp. Fig. 22 compares the WKB prediction of

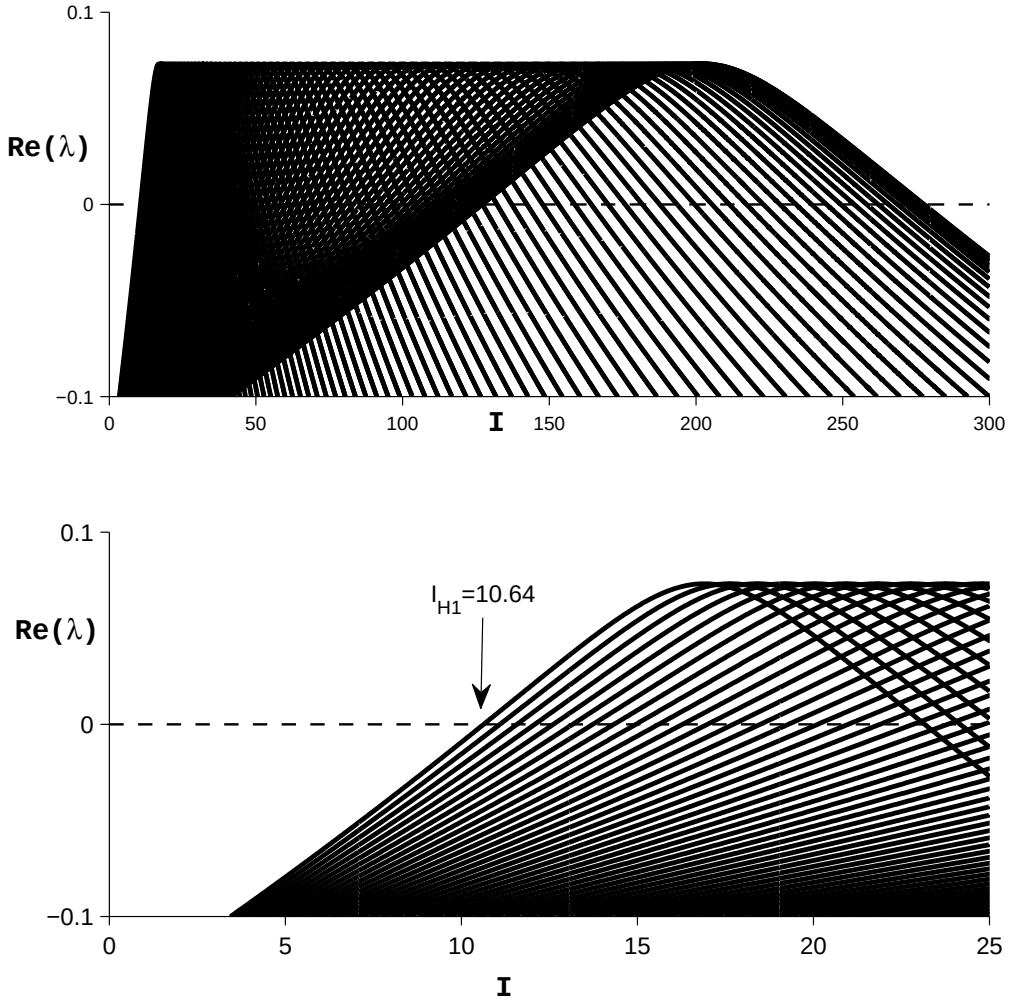

Figure 21: Spiny cable of length $L = 3$ with 75 uniformly distributed spines and uniform $G_{ss} = 0.02$. *Top*: Real portion of all eigenvalues with nonzero imaginary part. *Bottom*: Zoomed-in view.

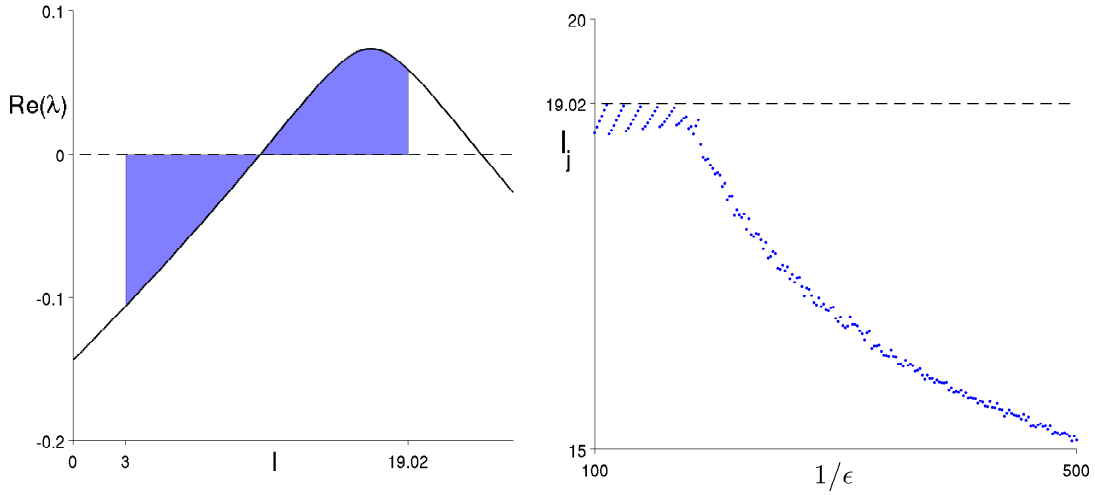

Figure 22: Uniform $G_{ss} = 0.02$. *Left*: WKB prediction of I_j in response to the slow ramp $I(t) = 3 + \epsilon t$, $\epsilon \to 0$. *Right*: I_j observed in numerical solutions.

$I_j = 19.02$ with the value of I_j as determined from numerical solutions of the PDE system, with I_j defined as the value of current at the moment the potential in some spine exceeds 0.5. From Fig. 23 one sees that the oscillations are predicted to arise almost exclusively at the current injection point, and that this is confirmed by the time courses of spinehead potential obtained from the numerical solution of the system for the particular ramp speed $\epsilon = 0.007$.

Intermediate spine stem conductance

I next investigated the effect of increasing the uniform spine stem conductances to $G_{ss} = 0.1$. As before, 75 compartments were used to perform the WKB analysis, and 150 (75 complex-conjugate pairs) of the resulting 225 eigenvalues have nonzero imaginary part for I in the range considered. Fig. 24 shows their real portions. All other eigenvalues are large and negative. One can see the following differences from Fig. 21 (low stem conductance): the Hopf points are lower, the maximal value attained by the real portions of the eigenvalues

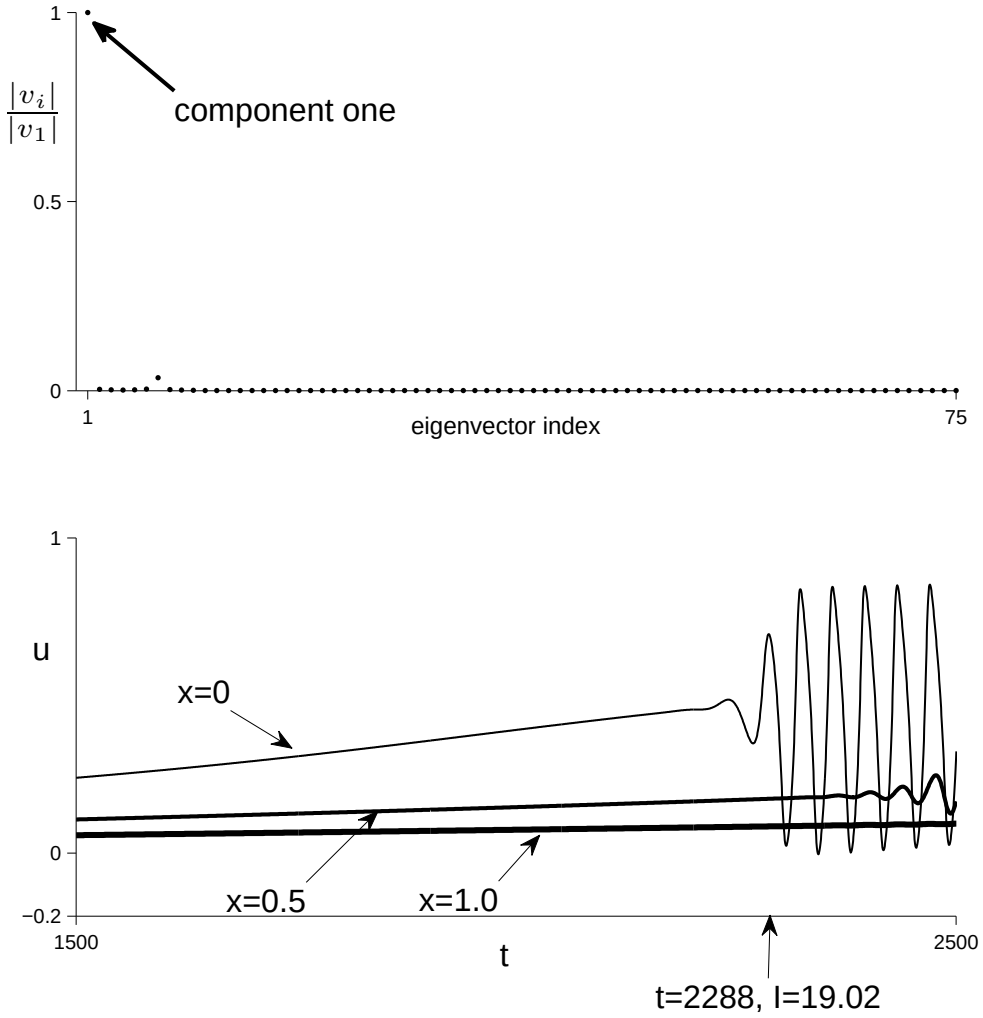

Figure 23: Uniform $G_{ss} = 0.02$. $I(t) = 3 + \epsilon t$. *Top*: WKB prediction of the location at which oscillations arise. *Bottom*: Time courses of spinehead potential. Ramp speed $\epsilon = 0.007$.

are smaller, and most interestingly, the eigenvalue responsible for instability is now distinct in shape from all the others.

I investigated the spiny cable response to the slow current ramp $I(t) = 2.25 + \epsilon t$, $\epsilon \to 0$. Fig. 25 compares the WKB prediction of $I_j = 6.205$ with the value of I_j as determined from numerical solutions of the PDE system, with I_j defined as the value of current at the moment the potential assigned to some grid point p exceeds the potential at grid point $p-2$ by at least 0.02. Prior to the onset of instability, the potential in the spineheads monotonically decreases with distance from the site of current injection; hence, if this condition is satisfied the system has become unstable. This criterion for defining I_j is preferable to setting an absolute threshold for u because the oscillations in spinehead potential are rather small in amplitude, due to the significant conductance load felt by the spines for $G_{ss} = 0.1$. Fig. 26 compares the WKB prediction that oscillations will arise at a distance of about $x = 0.13$ (corresponding to compartments 4 and 5) from the injection end of the cable with the numerical solution for the particular ramp speed $\epsilon = 0.0025$. This is interesting because the stem conductances are identical, the spines are uniformly distributed, and all cable parameters are uniform.

I next investigated the response to a slow linear ramp which starts at $I_0 = 1.25$, a unit further back from the Hopf point at $I \approx 3.915$. Fig. 27 compares the WKB prediction of $I_j = 9.01$ with the value of I_j as determined from numerical solutions of the PDE system, with I_j defined as the value of current at the moment the potential assigned to some grid point p exceeds the potential at grid point $p-2$ by at least 0.02. Fig. 28 compares the WKB prediction that oscillations will arise at a distance of about $x = 0.48$ (corresponding to compartment 12) from the injection end of the cable with

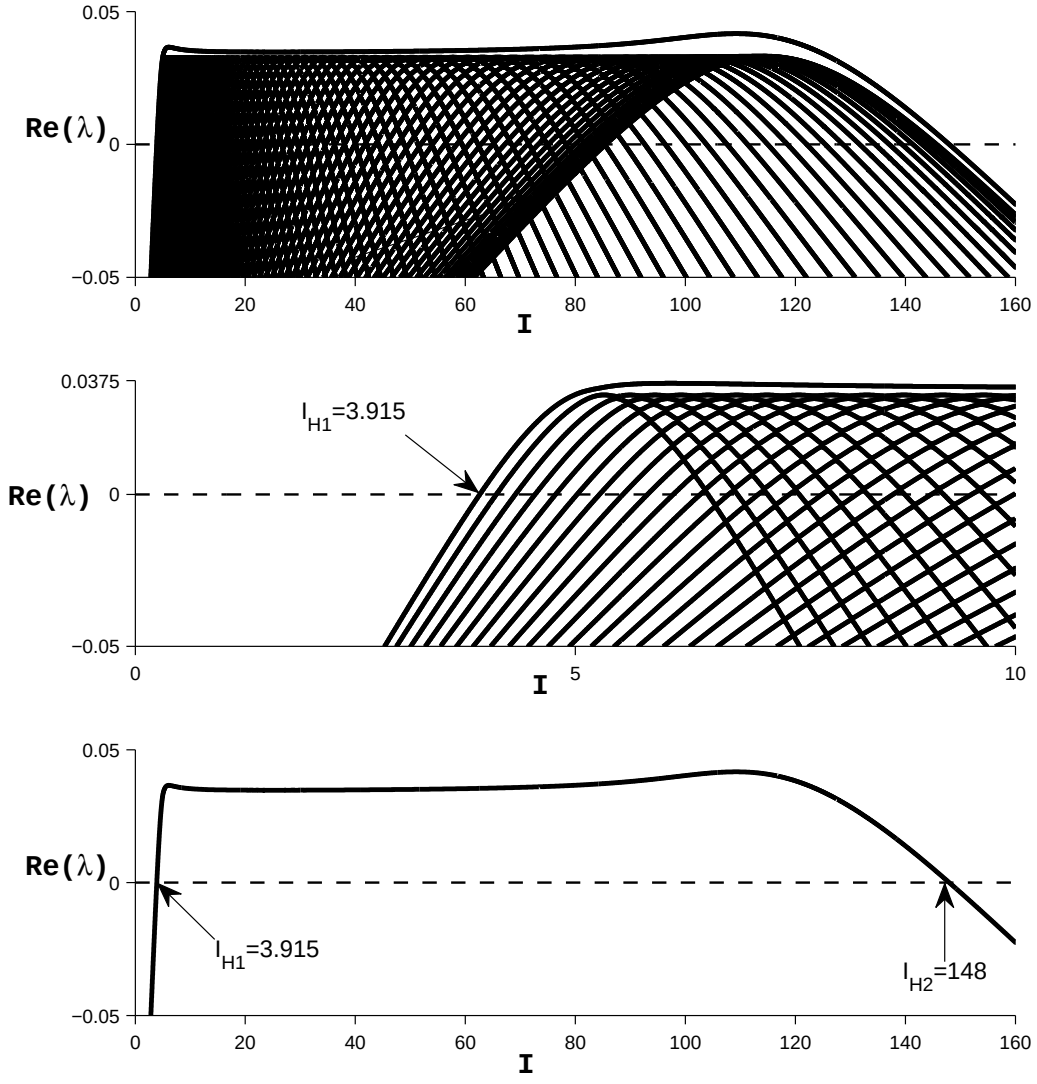

Figure 24: Spiny FitzHugh-Nagumo cable of length $L = 3$ with 75 uniformly distributed spines and uniform $G_{ss} = 0.1$. *Top*: $Re(\lambda)$ versus I. *Middle*: Zoom-in. *Bottom*: Eigenvalue satisfying onset condition.

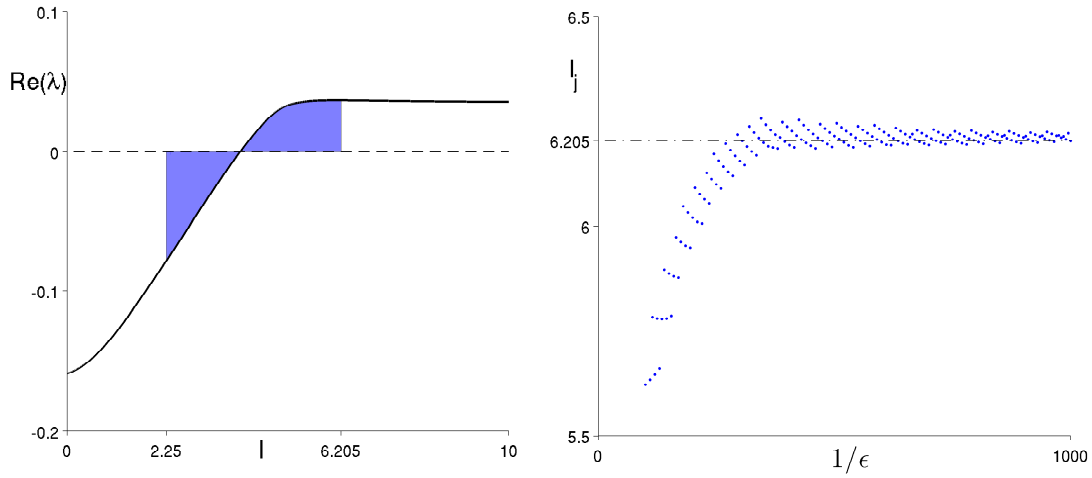

Figure 25: Uniform $G_{ss} = 0.1$. *Left*: WKB prediction of I_j in response to the slow current ramp $I = 2.25 + \epsilon t$, $\epsilon \to 0$. *Right*: I_j observed in numerical solutions.

the numerical solution for the particular ramp speed $\epsilon = 0.0025$.

Comparing the responses to the ramps $I(t) = 2.25 + \epsilon t$ and $I(t) = 1.25 + \epsilon t$, one sees that a smaller value of initial current results in a larger value of I_j, consistent with the memory effect. It also results in the oscillations arising further away from the current injection point, which fact is captured by $\vec{v}_j$: when $\vec{v}_j$ was evaluated at $I_j = 6.205$ in the previous trial, an inspection of its components indicated that it effected the largest change in spinehead potential variables associated with compartments 4 and 5. When evaluated at $I_j = 9.01$, the components of $\vec{v}_j$ are such that it effects the largest change in the spinehead potential variable associated with compartment 12.

Finally, I considered the nonlinear current ramp $I(t) = 2.25 + (\epsilon t)^2$, $\epsilon \to 0$. This is what is known as an accelerating current ramp, because the ramp speed $\frac{dI}{dt} = 2\epsilon^2 t$ is increasing with time. Recall that under the WKB prediction, I_j for a cable injected with the ramp $I = I_0 + g(\epsilon t)$, $\epsilon \to 0$ satisfies

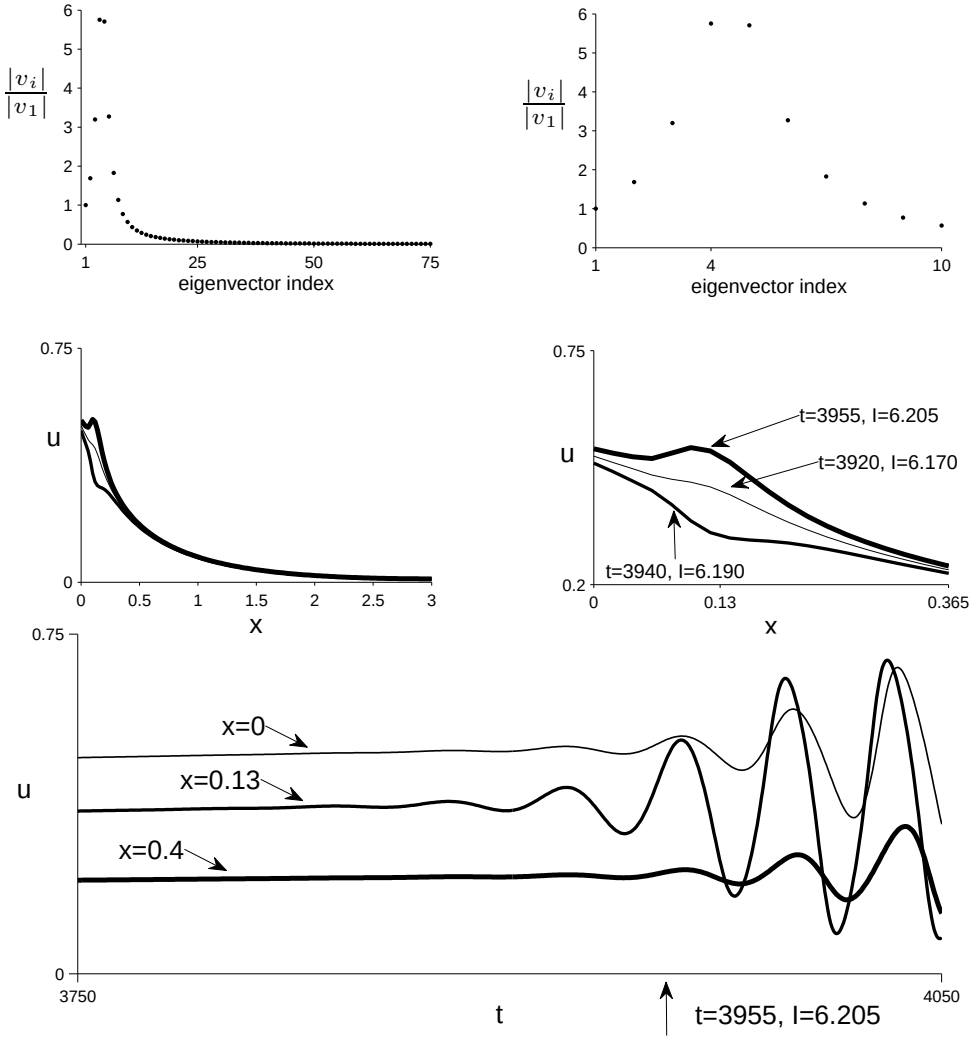

Figure 26: Uniform $G_{ss} = 0.1$. $I(t) = 2.25 + \epsilon t$. *Top*: WKB prediction for the location at which oscillations will arise. *Middle/Bottom*: Comparison with numerical solutions, for the ramp $\epsilon = 0.0025$.

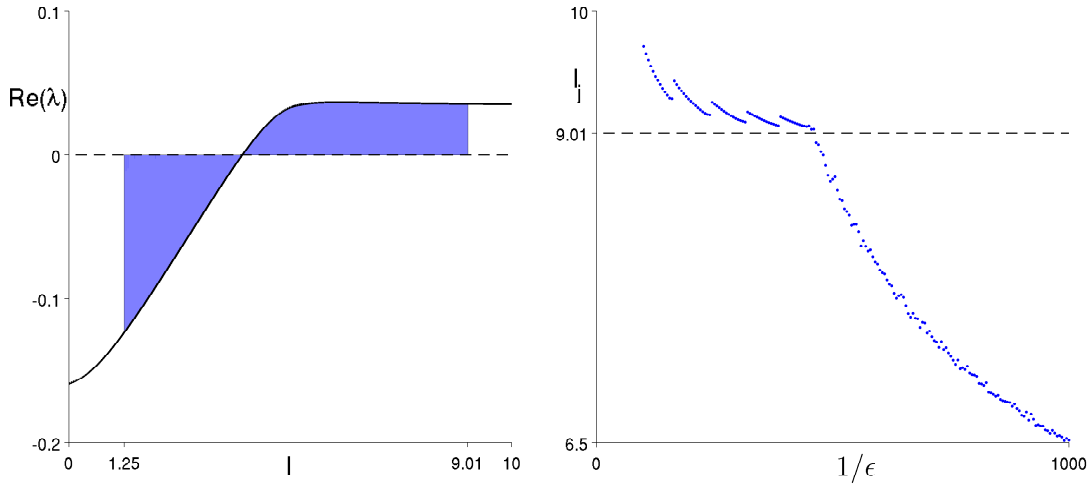

Figure 27: Uniform $G_{ss} = 0.1$. *Left*: WKB prediction of I_j in response to the slow current ramp $I = 1.25 + \epsilon t$, $\epsilon \to 0$. *Right*: I_j observed in numerical solutions.

$$\int_{I_0}^{I_j} [g^{-1}(I - I_0)]' Re(\lambda(I)) dI = 0.$$

For the ramp $I = 2.25 + (\epsilon t)^2$ this becomes

$$\int_{2.25}^{I_j} \frac{1}{\sqrt{I - 2.25}} Re(\lambda(I)) dI = 0.$$

For this nonlinear ramp, the function one must integrate is not simply $Re(\lambda(I))$, but a weighted version of it. Fig. 29 (left) shows the graphs of both $y = Re(\lambda(I))$ (dashed line) and $y = \frac{1}{\sqrt{I-2.25}} Re(\lambda(I))$ (solid line), and the WKB prediction of $I_j = 12.365$. Fig. 29 (right) shows I_j as determined from numerical solutions, using the same calling method as used for the previous two ramps. Fig. 30 compares the WKB prediction that oscillations will arise at a

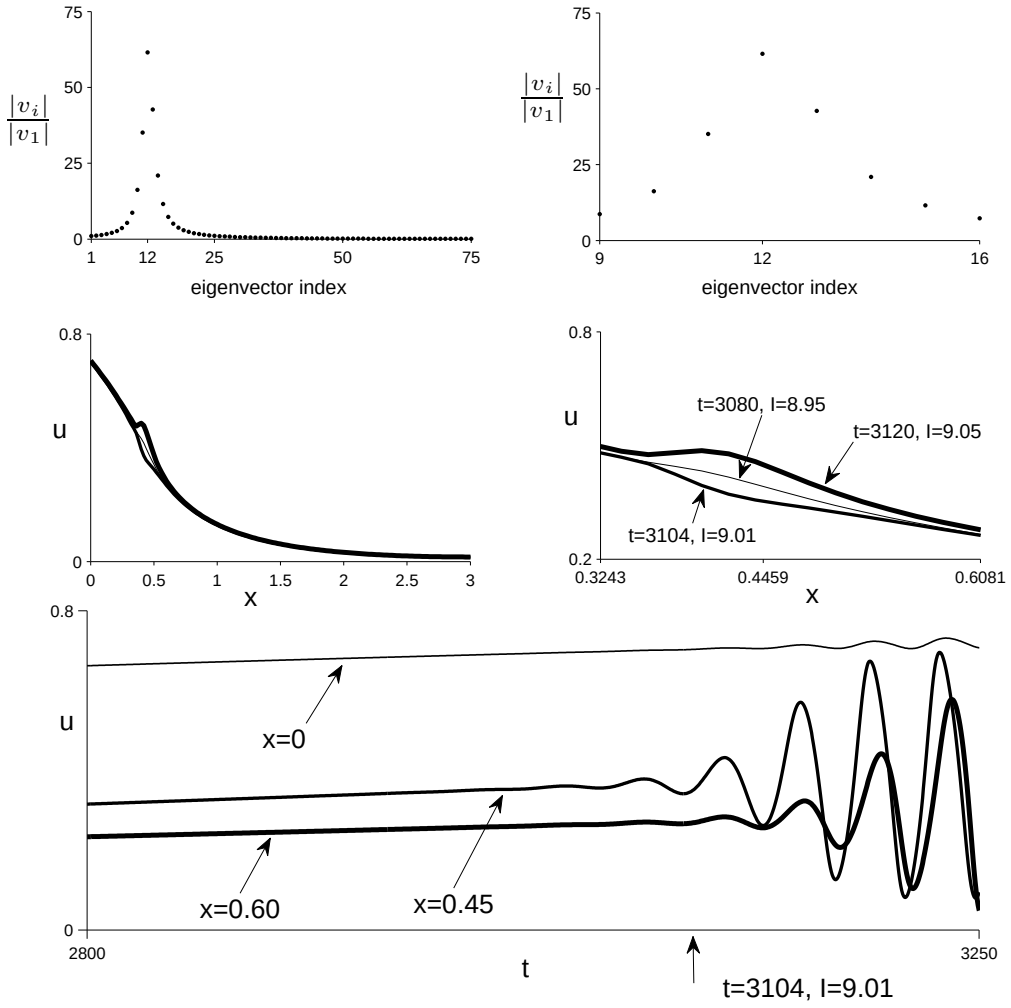

Figure 28: Uniform $G_{ss} = 0.1$. $I(t) = 1.25 + \epsilon t$. *Top*: WKB prediction for the location at which oscillations will arise. *Middle/Bottom*: Comparison with numerical solutions, for the ramp $\epsilon = 0.0025$.

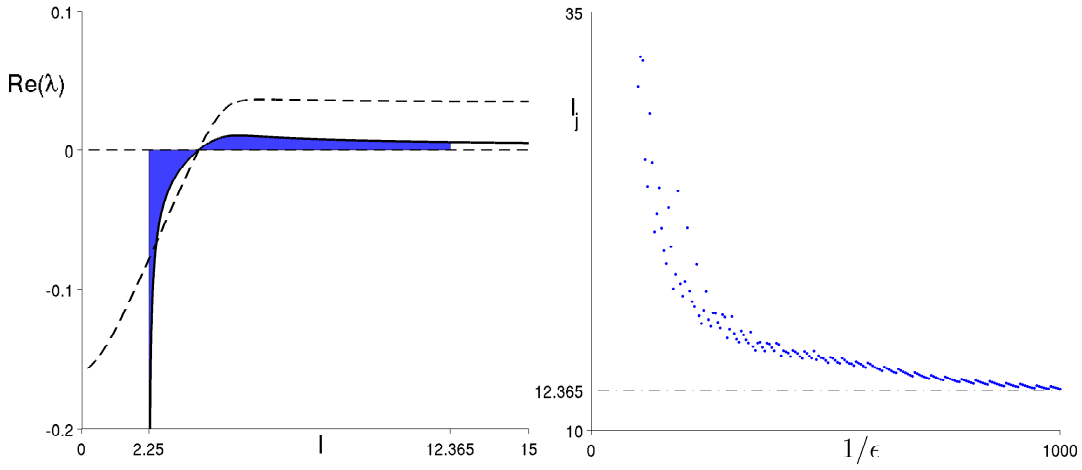

Figure 29: Uniform $G_{ss} = 0.1$. *Left*: WKB prediction of I_j in response to the slow accelerating current ramp $I = 2.25 + (\epsilon t)^2$, $\epsilon \to 0$. *Right*: I_j observed in numerical solutions.

distance of about $x = 0.69$ (corresponding to compartments 18 and 19) from the injection end of the cable with the numerical solution for $\epsilon = 0.001$.

Of the three ramps considered, the accelerating ramp results in the largest apparent firing threshold, and the most distal oscillations.

High spine stem conductance

I then increased the spine stem conductances still further, to $G_{ss} = 0.35$. Increasing G_{ss} tends to decrease the real portions of the eigenvalues due to increased coupling to the passive cable load, and for this value of conductance the cable with 75 spines is not excitable (the Hopf points coalesce and vanish). Hence, I increased the number of spines to 360; a uniform spine density of $\bar{n} = 120$ was used for these trials. A larger number of compartments were needed for the eigenvalue picture to stabilize; I used 100 compartments, resulting in 300 eigenvalues. Of them, 200 (100 complex-conjugate pairs) have nonzero imaginary part for I in the range considered. Fig. 31 shows their real portions.

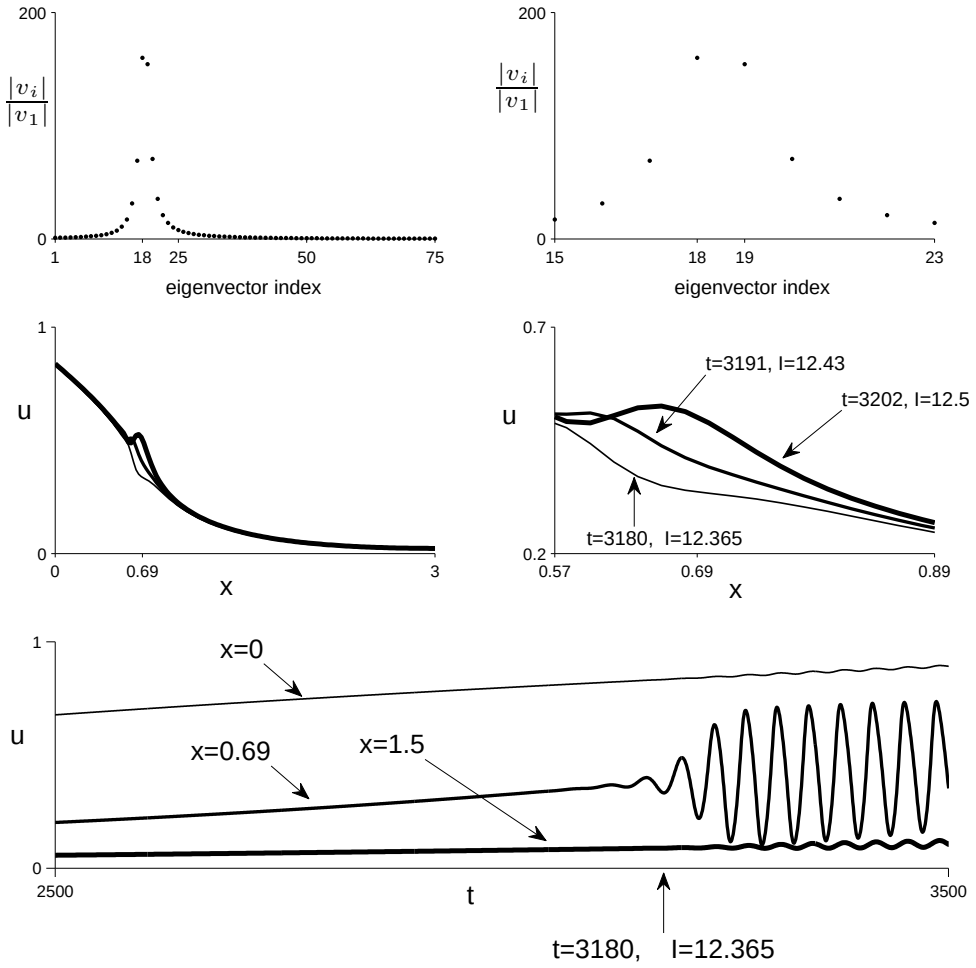

Figure 30: Uniform $G_{ss} = 0.1$. $I(t) = 2.25 + (\epsilon t)^2$. *Top*: WKB prediction for the location at which oscillations will arise. *Middle/Bottom*: Comparison with numerical solutions, for the ramp $\epsilon = 0.001$.

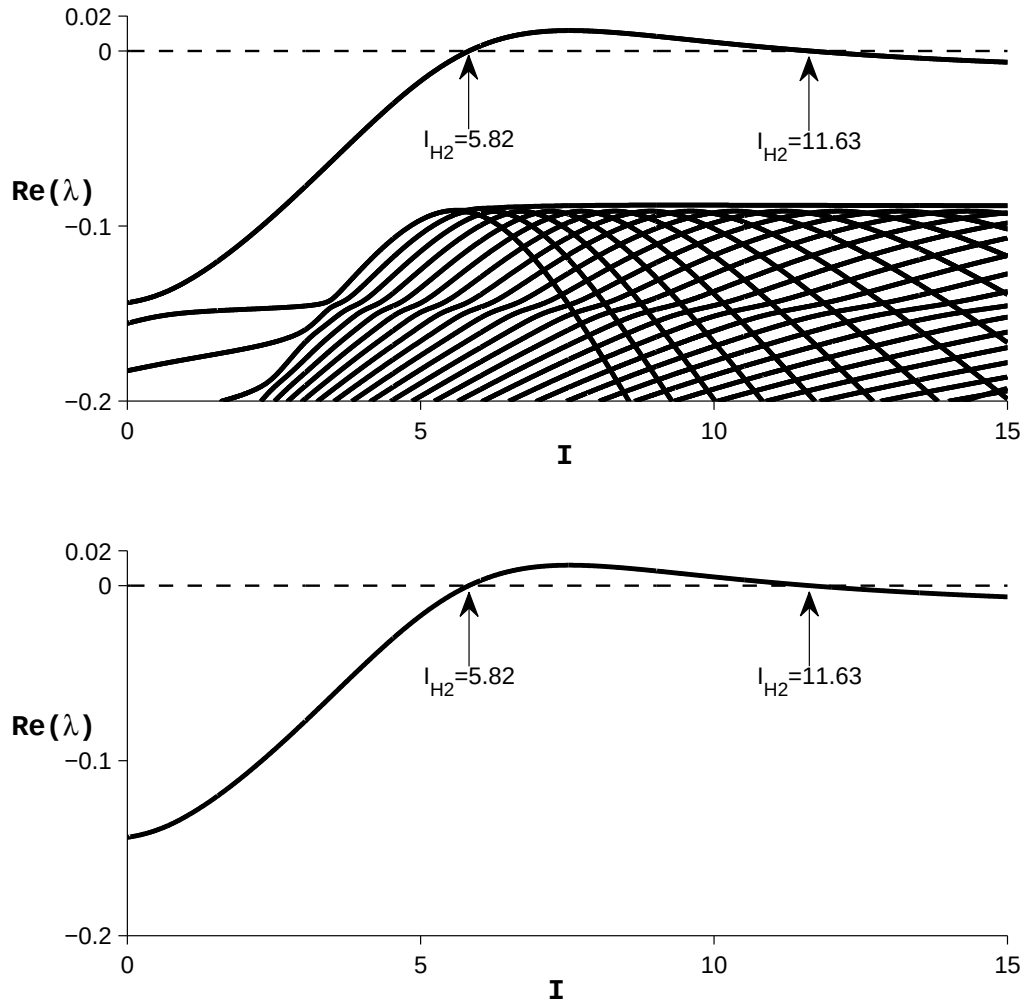

Figure 31: Spiny FitzHugh-Nagumo cable of length $L = 3$ with 360 uniformly distributed spines and uniform $G_{ss} = 0.35$. *Top*: $Re(\lambda)$ vs. I. *Bottom*: $Re(\lambda)$ vs. I for the only eigenvalue crossing imaginary axis.

As in previous cases, all other eigenvalues are large and negative. Only one complex conjugate pair of eigenvalues attains positive real part for this large value of G_{ss}.

Figures 32 and 33 compare the WKB prediction for I_j with numerical

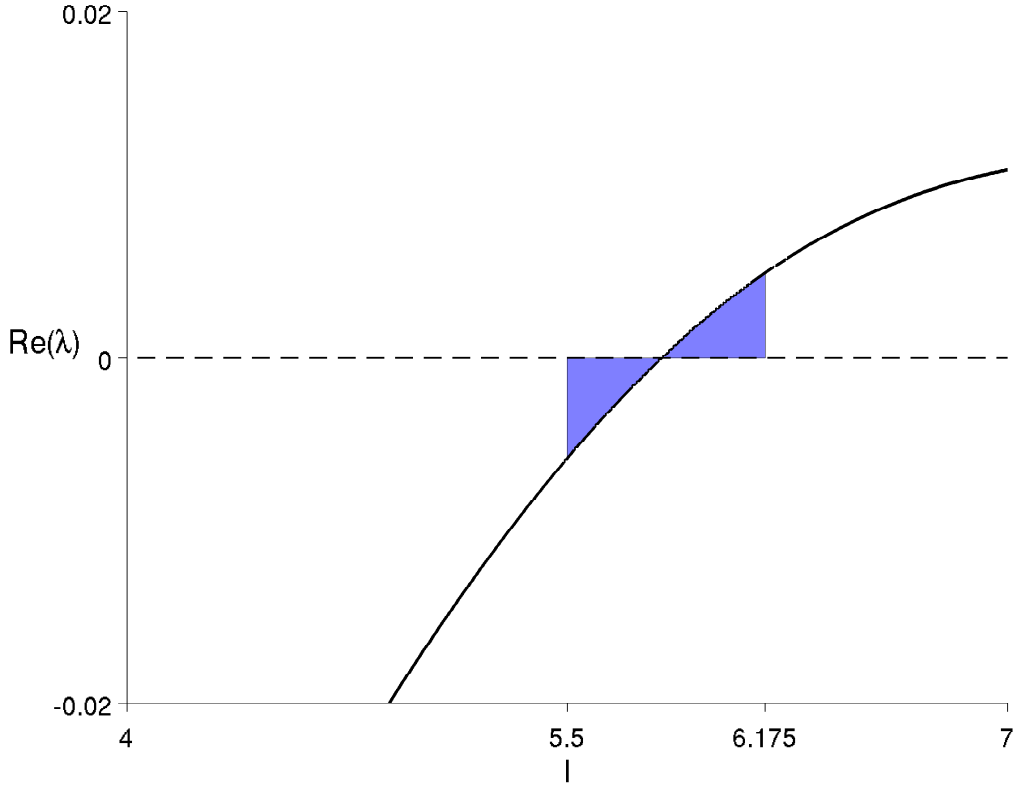

Figure 32: Uniform $G_{ss} = 0.35$. WKB prediction of I_j in response to the slow current ramp $I = 5.5 + \epsilon t$, $\epsilon \to 0$.

solutions of the spiny cable response to the ramp $I(t) = 5.5 + \epsilon t$ as $\epsilon \to 0$. I_j determined from numerical solutions is defined as the value of current when some spine has $u > 0.465$. The numerically determined I_j slightly overshoots the WKB prediction, and this is due to the very small value of $Re(\lambda)$ at I_j, as discussed in the previous chapter. Fig. 34 confirms the prediction that upon reaching $I = 6.175$, oscillations arise over a region of the cable from about $x = 0$ to $x = 0.75$, with amplitude falling off as distance from the injection point increased. When the stem conductance is lower, the oscillations are much more localized.

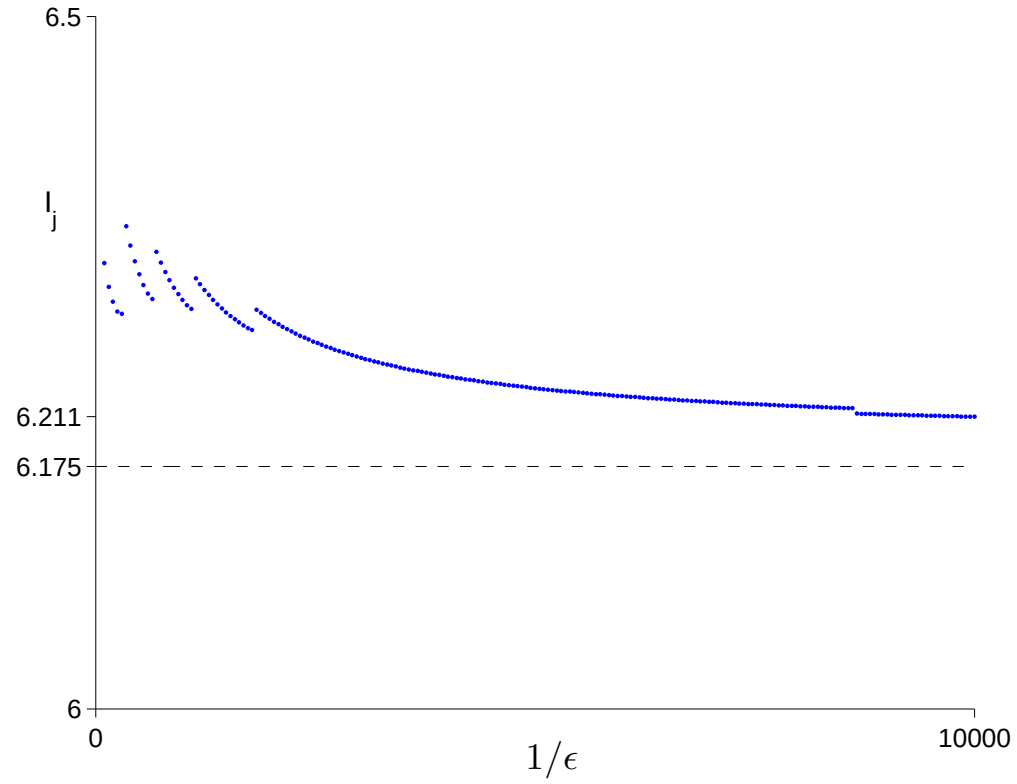

Figure 33: Uniform $G_{ss} = 0.35$. I_j observed in numerical solutions of the spiny cable's response to the slow current ramp $I(t) = 5.5 + \epsilon t$.

Finally, I considered the cable response to a ramp with a somewhat smaller initial current, $I(t) = 4.25 + \epsilon t$. Fig. 35 compares the WKB prediction for I_j with numerical solutions. I_j is defined as the value of current when some spine has $u > 0.685$. From Fig. 36 one sees that the component of $\vec{v_j}$ with the largest modulus corresponds to the cable location $x = 0.24$, and hence has shifted away from the injection point. However, the maximum modulus is only about a factor of 2 greater than the modulus corresponding to the injection point; hence, the amplitude of oscillations away from the slowly-varying solution near $x = 0.24$ is expected to be only slightly larger than the

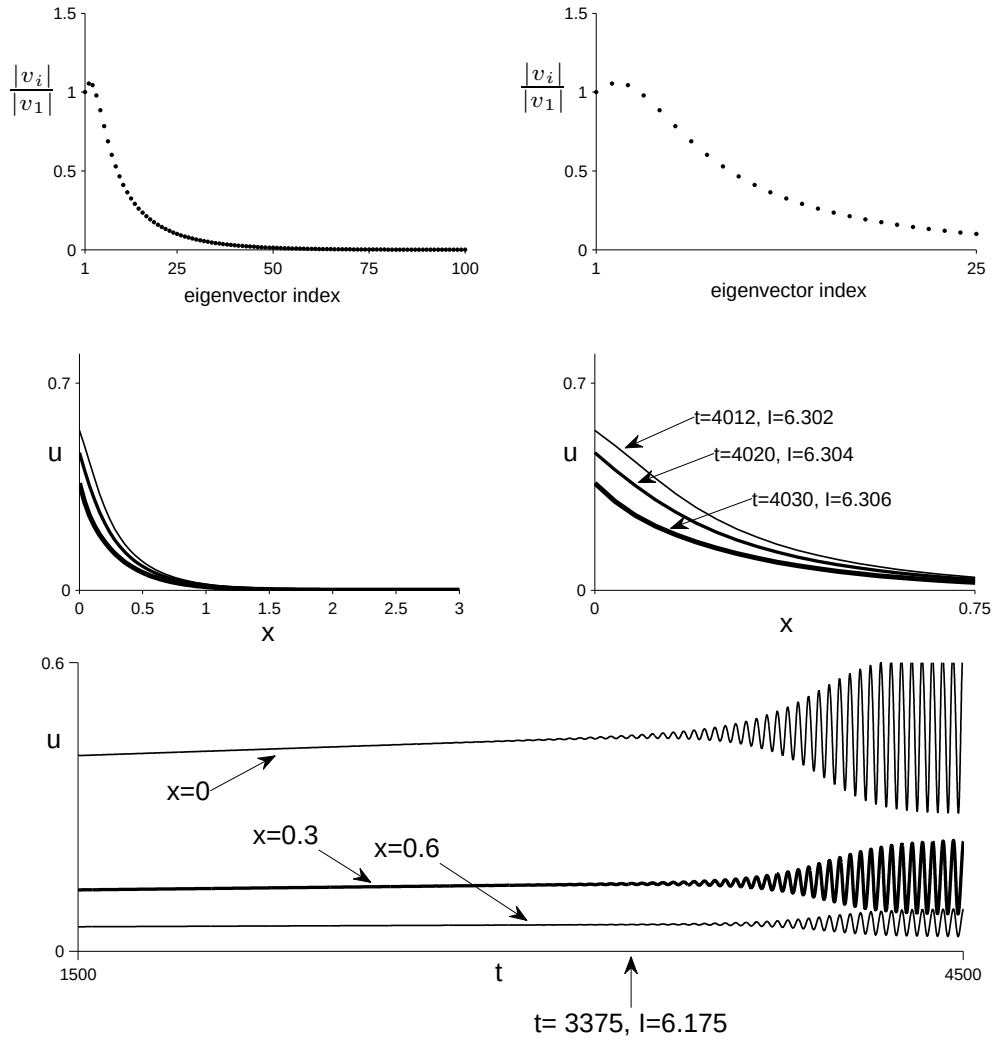

Figure 34: Uniform $G_{ss} = 0.35$. $I(t) = 5.5 + \epsilon t$. *Top*: WKB prediction for the location at which oscillations will arise. *Middle/Bottom*: Comparison with numerical solutions, for the ramp $\epsilon = 0.0002$.

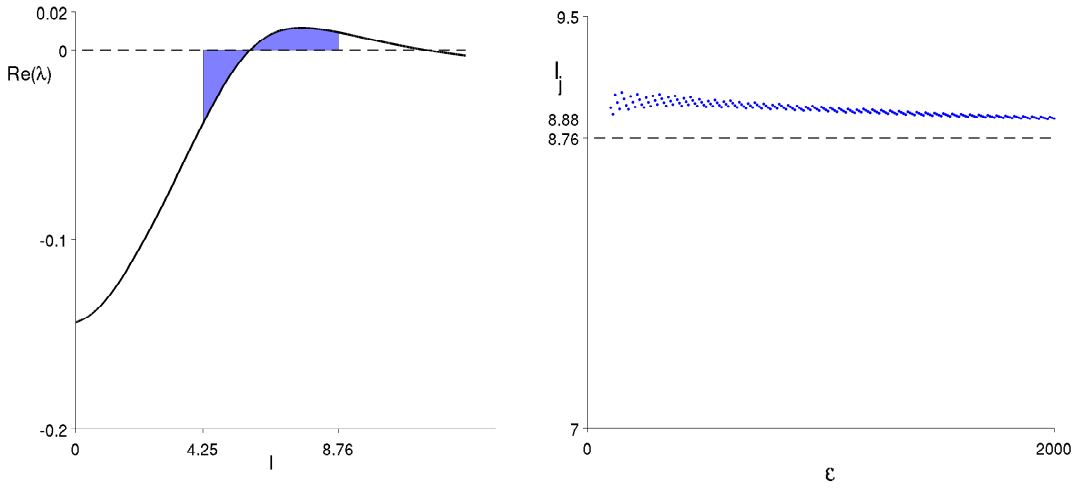

Figure 35: $G_{ss} = 0.35$. *Left*: WKB prediction of I_j in response to the slow current ramp $I(t) = 4.25 + \epsilon t$, $\epsilon \to 0$. *Right*: I_j observed in numerical solutions.

amplitude of oscillations near $x = 0$. Numerical simulations confirmed this.

From Fig. 32 and 35 one sees that $I_j = 6.175$ is quite close to the first Hopf point, while $I_j = 8.76$ is approximately halfway between the two Hopf points; however, little difference exists between the moduli of components of the vector $\vec{v_j}$ evaluated at the two values of I. Although the cable location corresponding to the maximum-amplitude oscillations does shift away from the injection site, it does not shift far, and the maximum amplitude is only about a factor of 2 larger than at the injection site.

3.4 Discussion

The spiny cable I considered is a system consisting of two components, an excitable component (the spines) and a passive component (the cable shaft). The stem conductance G_{ss} modulates the degree of electrical coupling between these components. Furthermore, since the spines communicate only diffusively via the cable, G_{ss} determines the degree of this communication. For the case

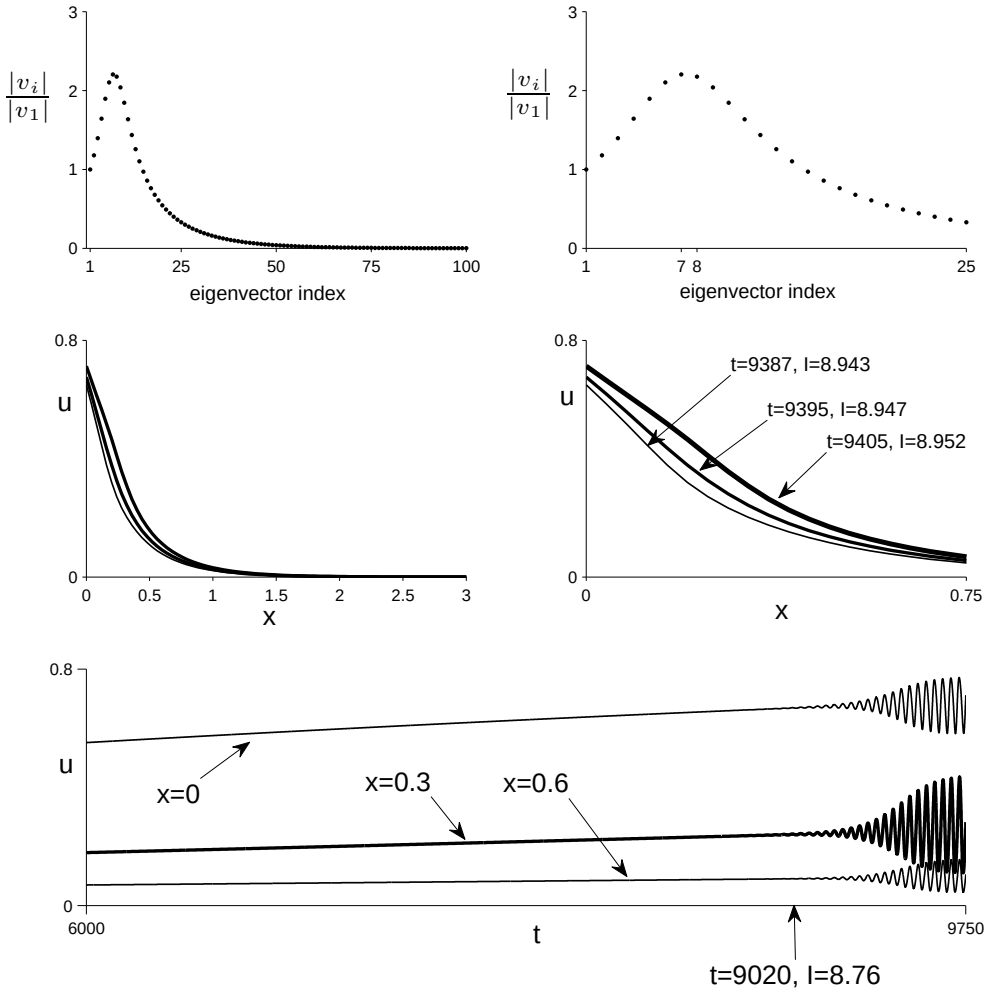

Figure 36: $G_{ss} = 0.35$. $I(t) = 4.25 + \epsilon t$. *Top*: WKB prediction for the location at which oscillations will arise. *Middle/Bottom*: Comparison with numerical solutions, for the ramp $\epsilon = 0.0005$.

$G_{ss} = 0.02$, 75 of the 225 eigenvalues of the compartmentalized system are real and negative, while the other 150 (75 complex conjugate pairs) have nonzero imaginary part and have a functional dependence $Re(\lambda(I))$ on I like that seen for the 2-variable FitzHugh-Nagumo model. This suggests that $G_{ss} = 0.02$ (low stem conductance) is small enough that the spines behave like isolated FitzHugh-Nagumo systems, and that each of the 75 complex conjugate pairs of eigenvalues is almost exclusively associated with a single spine, while the 75 real, negative eigenvalues are associated with the passive cable. Eigenvector inspection confirmed this, and indicated that spine one is associated with the first eigenvalue pair to cross the imaginary axis as I increases, spine two is associated with the second eigenvalue pair to cross the imaginary axis, etc. The graphs of $Re(\lambda(I))$ for the eigenvalues crossing the imaginary axis appear to be related to each other through a horizontal stretch; this reflects the fact that some current leaks out of the passive cable membrane en route to the spines, and this loss is greater for spines further from the site of current injection.

When I increase G_{ss} to 0.1 (intermediate stem conductance), the eigenvalue pair $\lambda(I)$ governing stability becomes functionally distinct from all others. I call the eigenvector (technically, one of the two complex conjugate eigenvectors) associated with this eigenvalue pair $\vec{v}_j(I)$. In contrast to the situation for $G_{ss} = 0.02$, $\vec{v}_j(I)$ is not overwhelmingly associated with one spine, reflecting the fact that a larger stem conductance results in greater communication among the spines. However, for each value of I the eigenvector $\vec{v}_j$ is much more strongly associated with one particular spine (or a few adjacent spines) than with all the others, as indicated by an inspection of its components. At $I_{H1} = 3.915$, the dominant spine is the one at the site of current injection. I found that as I increases, the location of the dominant spine moves toward the

other end of the cable. Hence, the greater the amount by which I_j exceeds the first Hopf point for a given current ramp, the farther from the site of current injection oscillations arise. These results suggest that for $G_{ss} = 0.1$ the spines maintain some degree of independence: each has an interval of I (current injected into the cable), determined by its position, over which it fires, and as I_j moves away from the first Hopf point the identity of the spine into whose range of firing I_j squarely falls shifts away from the injection site.

For the stem conductance $G_{ss} = 0.35$ (high stem conductance), the spines feel heavily the passive cable's load; I increased the number of spines to 360 because at this stem conductance the system with 75 spines is not excitable. For 360 uniformly distributed spines and $G_{ss} = 0.35$, the range of repetitive firing is $[5.82, 11.63]$; the second Hopf point is an order of magnitude smaller for this conductance than for the cases of $G_{ss} = 0.1$ and $G_{ss} = 0.02$, even though many more spines are present in this case. It may be that the cable load felt by the spines is large enough that only currents I which fall into the excitable ranges for a large number of spines can excite the system, and adjacent spines located near the injection point have the greatest overlap in their ranges of excitability. In contrast, when $G_{ss} = 0.02$, the spines are nearly decoupled from the cable, and as long as even one spine receives current in its excitable range the system experiences sustained oscillations. For example, I near the second Hopf point at $I_{H2} = 277.2$ might excite only a few spines near the far end of the cable.

I found that for the case $G_{ss} = 0.35$, when the system becomes unstable significant oscillations in spinehead potential arise over a large range of the cable, for both $I_j = 6.175$ and $I_j = 8.76$. Although $I_j = 8.76$ is closer to the second Hopf point than the first, the location of the largest-amplitude

oscillations only shifts to $x = 0.24$ on a cable of length $L = 3$. This supports the idea that the excitable range of $[5.82, 11.63]$ is associated only with those spines close to the site of current injection.

Chapter 4

RESPONSE OF FITZHUGH-NAGUMO AND HODGKIN-HUXLEY AXONAL CABLES TO A SLOW CURRENT RAMP

4.1 FitzHugh-Nagumo axonal cable

I now consider the FitzHugh-Nagumo axonal cable, where the ion channels responsible for the generation of action potentials are embedded in the shaft membrane. The model equations are as follows:

$$\frac{\partial u}{\partial t} = \frac{\partial^2 u}{\partial x^2} - f(u) - w \tag{4.1}$$

$$\frac{\partial w}{\partial t} = b(u - \gamma w). \tag{4.2}$$

I consider a FitzHugh-Nagumo cable of dimensionless length L with current $I(t) = I_0 + \epsilon t$ injected into one end and the other end sealed to current. The boundary conditions are

$$\frac{\partial V}{\partial X}(0,t) = -I(t) \tag{4.3}$$

$$\frac{\partial V}{\partial X}(L,t) = 0. \tag{4.4}$$

As with the spiny cable, I compartmentalize in order to apply the WKB analysis. Let the first compartment ($i = 1$) correspond to the end at which current is injected. For n compartments, the equations governing compartment i, $1 \leq i \leq n$ are

$$\dot{u_i} = -f(u_i) - w_i + \frac{u_{i-1} - 2u_i + u_{i+1}}{\Delta X^2} \tag{4.5}$$

$$\dot{w_i} = b(u_i - \gamma w_i) \tag{4.6}$$

where ΔX is the length of one compartment. The boundary conditions are handled with "ghost" compartments:

$$u_0 = u_2 + 2\Delta XI \tag{4.7}$$

$$u_{n+1} = u_{n-1}. \tag{4.8}$$

Each compartment has associated with it two variables, u and w. For convenience when analyzing eigenvector components, I choose to arrange the equations such that for the $i'th$ compartment,

$$\dot{u}_i = x_i \tag{4.9}$$

$$\dot{w}_i = x_{i+n}. \tag{4.10}$$

Hence, the approximating ODE to which I apply the WKB analysis is $2n$-dimensional. The first n variables correspond to the potential in the cable, and the second n variables are the slow recovery variables.

4.2 Results: FitzHugh-Nagumo axonal cable

Response to a slow current ramp

For the parameters used by Baer and Gaekel [2], $a = 0.02$, $b = 0.05$, $\gamma = 0.04$, I investigated the response of a FitzHugh-Nagumo cable of length $L = 2.5$ to slow linear current ramps injected at one end, while the other end is sealed to current. I used 125 compartments to perform the WKB analysis, resulting in 250 eigenvalues. Of them, only one (complex-conjugate) pair of eigenvalues had nonzero imaginary part. Figure 37 shows the real portion of this pair. All other eigenvalues are large and negative.

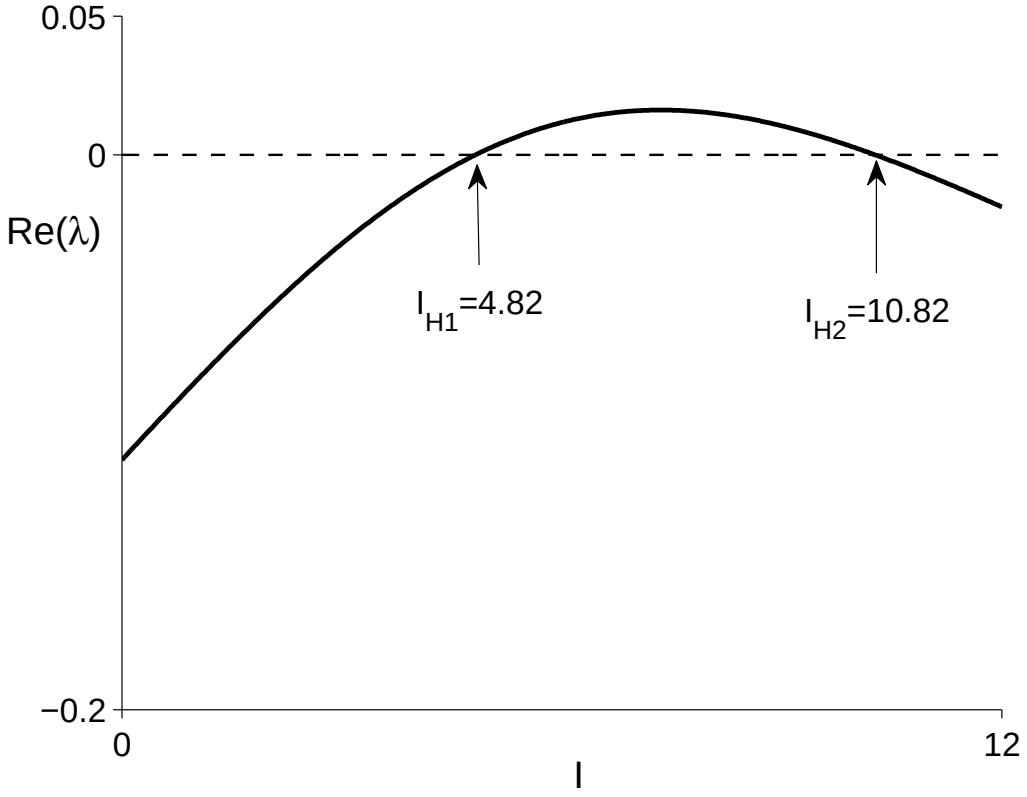

Figure 37: FitzHugh-Nagumo cable of length $L = 2.5$, where $a = 0.02$, $b = 0.05$ and $\gamma = 0.04$. Shown is the real portion of the one complex-conjugate eigenvalue pair with nonzero imaginary part.

Figure 38 compares the WKB prediction for I_j in response to the slow current ramp $I(t) = 3.5 + \epsilon t$, $\epsilon \to 0$ with that observed in numerical solutions of equations (4.1-4.4), with I_j defined as the value of current at the moment the potential at some point in the cable exceeds 0.75. I note that there appear to be two plots of I_j versus $1/\epsilon$, but this is not the case. This peculiarity is the result of the number of oscillations the system undergoes before the threshold is attained. If more data points had been collected, the usual jitter pattern would be seen. Figure 39 compares the WKB prediction that oscillations will arise all along the cable with the numerical solution for the particular ramp

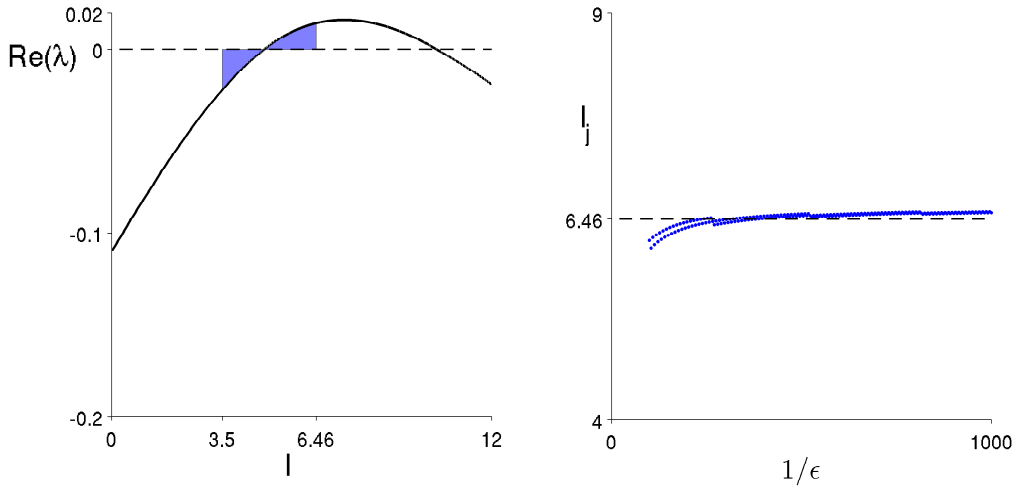

Figure 38: FitzHugh-Nagumo cable of length $L = 2.5$. *Left*: WKB prediction of I_j in response to the slow current ramp $I = 3.5 + \epsilon t$, $\epsilon \to 0$. *Right*: I_j observed in numerical solutions.

speed $\epsilon = 0.001$. Consistent with the WKB prediction, oscillations arise all along the cable once $I_j = 6.46$ is attained, and there is little difference in amplitude for different points along the cable.

The next ramp I considered was $I(t) = 2.5 + \epsilon t$, $\epsilon \to 0$. Fig. 40 compares the WKB prediction for I_j in response to the slow current ramp $I(t) = 2.5+\epsilon t$, $\epsilon \to 0$ with that observed in numerical solutions, with I_j defined as the value of current at the moment the potential at some point in the cable exceeds 0.93. The jitter pattern seen differs from that in Fig. 38 in a way that suggests fewer data points were used. This is not the case, and is due to the fact that the frequency of oscillations away from the slowly-varying solution depends on I. Fig. 41 compares the WKB prediction that oscillations will arise all along the cable with the numerical solution for the particular ramp speed $\epsilon = 0.001$.

Although this second ramp results in $I_j = 8.58$, a value closer to the second Hopf point than the first, there is no difference in the location at which

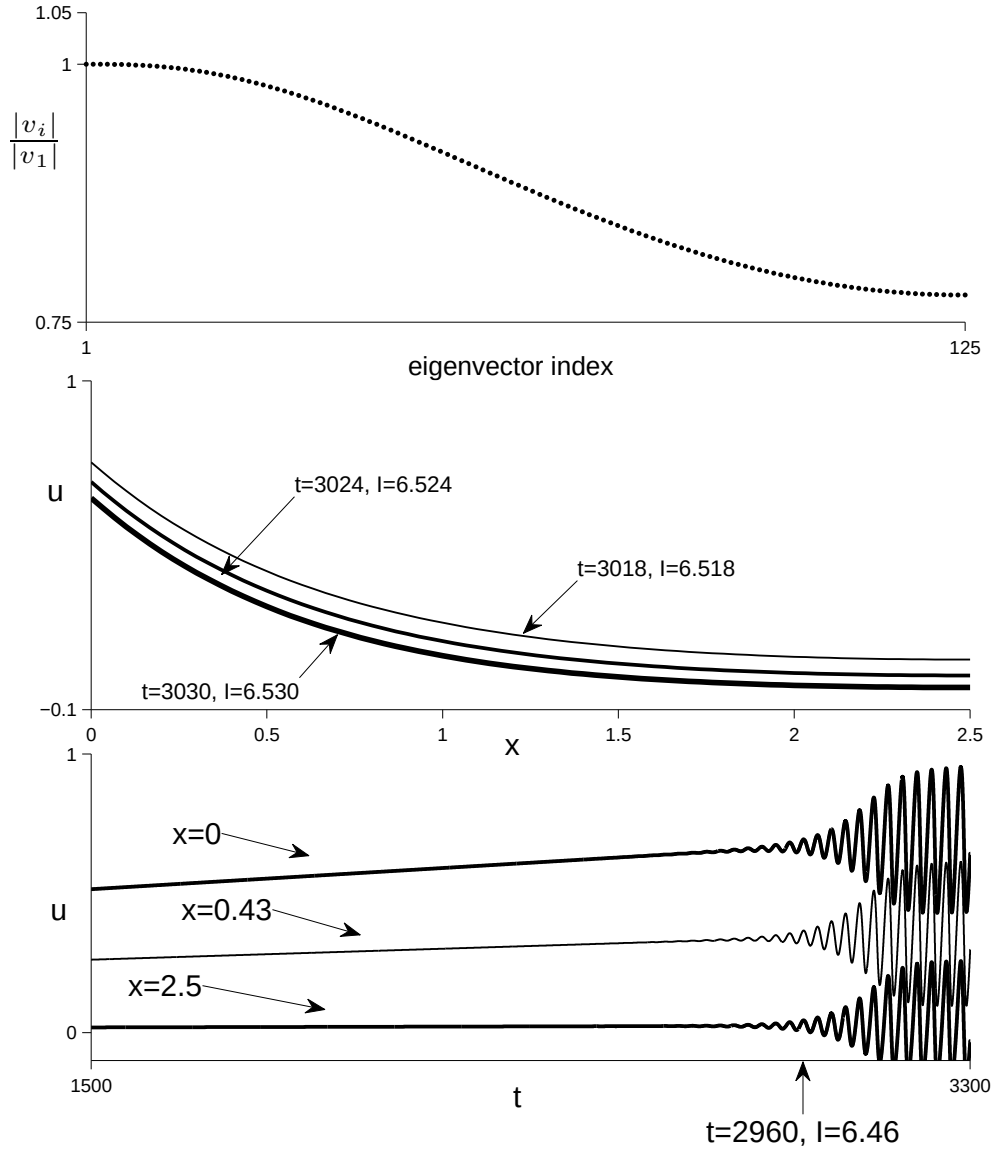

Figure 39: $L = 2.5$ cable. $I(t) = 3.5 + \epsilon t$. *Top*: The WKB method predicts that oscillations will arise over the full length of the cable. *Middle/Bottom*: Numerical solutions for $\epsilon = 0.001$

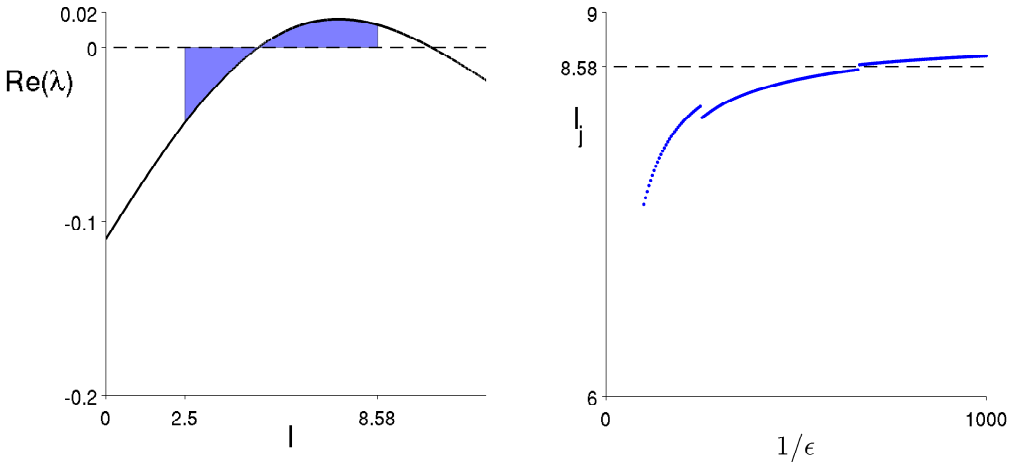

Figure 40: $L = 2.5$ cable. *Left*: WKB prediction of I_j in response to the slow current ramp $I = 2.5 + \epsilon t$, $\epsilon \to 0$. *Right*: I_j observed in numerical solutions.

oscillations arise; oscillations still arise all along the cable once I_j is attained.

Complete accommodation to a slow linear current ramp from $I_0 = 0$.

Hodgkin and Huxley [11] speculated that for a sufficiently slowly rising current, their model would never fire, regardless of how large the value of current became. I call this phenomenon "complete accommodation." To demonstrate complete accommodation in the FitzHugh-Nagumo cable, I used the FitzHugh-Nagumo parameters used for the spiny cable, $a = 0.14$, $b = 0.05$, $\gamma = 2.54$; these parameter values reduce the interval for repetitive firing, i.e. move the upper and lower Hopf points closer together.

Fig. 42 shows I_j versus the inverse ramp speed ϵ^{-1} obtained from numerical solutions for cable lengths $L = 0.5$, $L = 1$, $L = 2.5$, and $L = 3$. As one moves to the right across the graph, $\epsilon \to 0$ and one enters the regime of validity for the WKB approximation. For the two shorter cables, $L = 0.5$ and 1, the WKB method predicts a value of I_j at which the cable will become unstable, and numerical solutions confirmed this. However, for the two longer

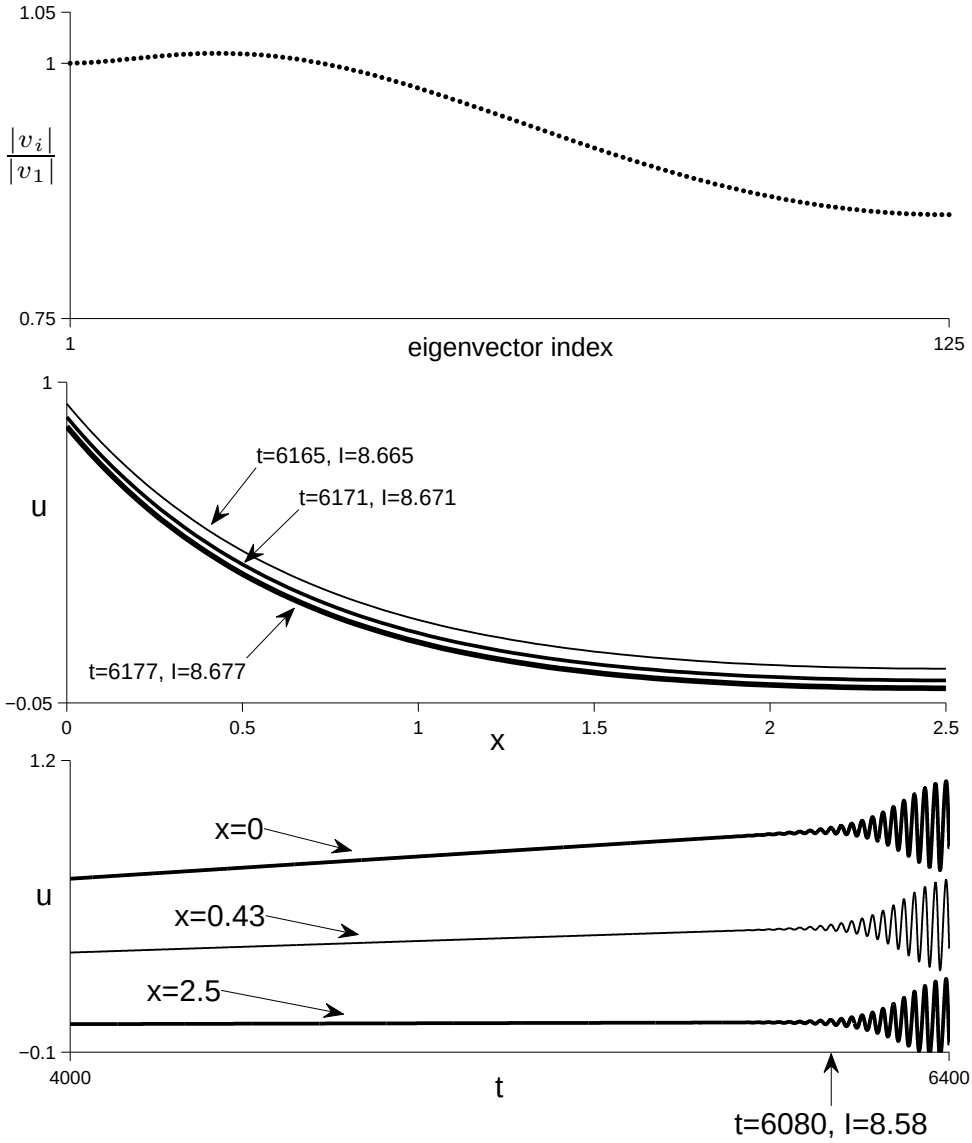

Figure 41: Cable length $L = 2.5$. $I(t) = 2.5 + \epsilon t$. *Top*: The WKB method predicts that oscillations will arise over the full length of the cable. *Middle/Bottom*: Numerical solutions for $\epsilon = 0.001$

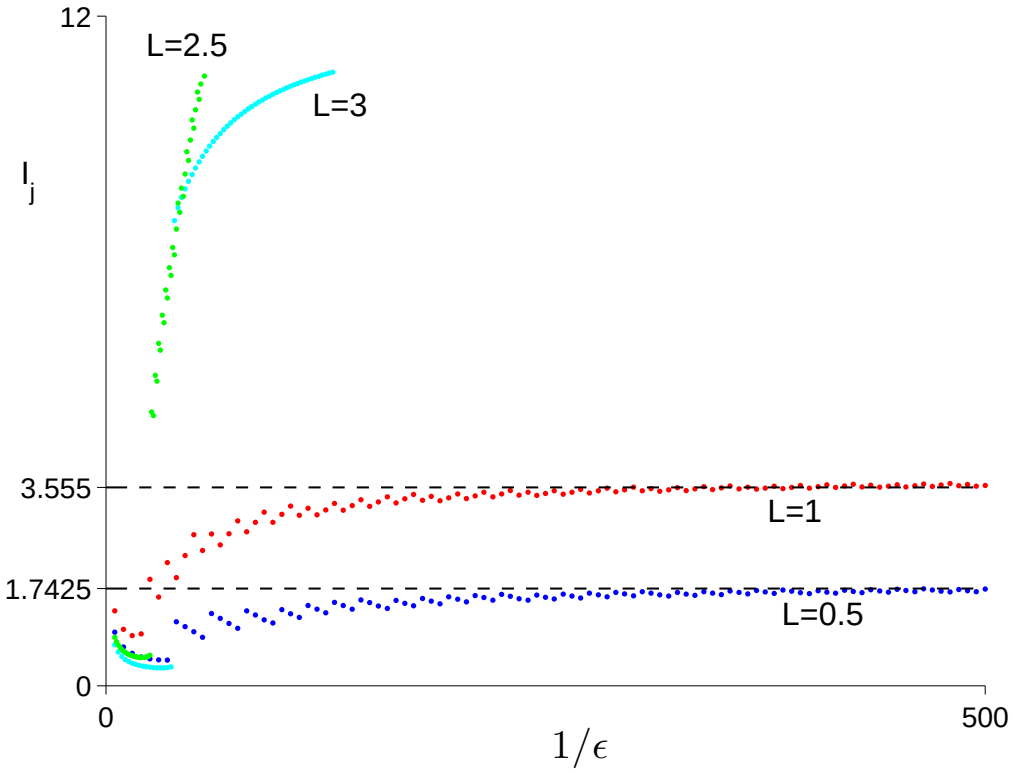

Figure 42: I_j observed in numerical solutions of the axonal cable PDE subject to the ramp $I(t) = \epsilon t$ versus inverse ramp speed, for FitzHugh-Nagumo cables of several lengths.

cables, $L = 2.5$ and 3, the WKB method predicts that the cable will never go unstable no matter how large the injected current becomes. Numerical solutions confirmed this: as $1/\epsilon$ becomes large, one enters into the WKB regime and the graph ceases to exist (no I_j is observed by the time the second Hopf point is passed). This suggests the existence of a minimal cable length for complete accommodation.

The dependence of complete accommodation on cable length can be understood from Fig. 43. Increasing the cable length causes the graph of $Re(\lambda)$ to change in such a way that it is impossible for the WKB onset condition to

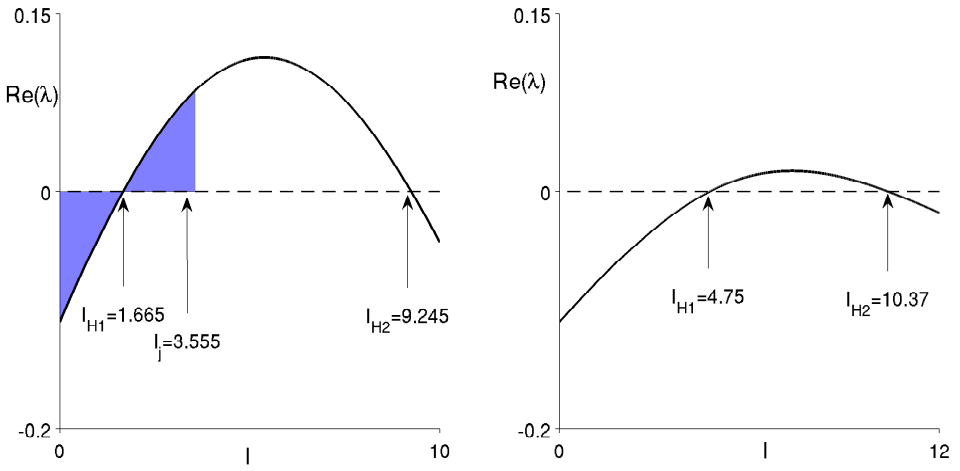

Figure 43: FitzHugh-Nagumo cable with parameters $a = 0.14$, $b = 0.05$, $\gamma = 2.54$. $Re(\lambda)$ versus I. *Left*: $L = 1$. I_j is predicted to exist. *Right*: Cable of length $L = 2.5$. Complete accommodation predicted.

be satisfied.

4.3 Complete accommodation to a slow linear current ramp from $I_0 = 0$ in the Hodgkin-Huxley axonal cable

I then turned to the Hodgkin-Huxley cable. In the following equations, V corresponds to electrical potential, and m, n, and h are "gating variables" which govern the opening and closing of sodium and potassium ion channels embedded in the cable membrane. The gating variables vary between 0 and 1. $\bar{g}_{Na}$ and $\bar{g}_K$ are the maximal specific conductances associated with the sodium and potassium ion channels. g_L is the specific conductance associated with the leakage current and is due to the passive properties of the cable membrane. E_{Na}, E_K, and E_L are the reversal potentials for the sodium, potassium, and leakage currents. C_m is the specific membrane capacitance, d is the cable diameter, and R_i is the axial resistivity. The equation for V is a current-balance equation. The sodium and potassium channels are modeled

as voltage-gated, which is captured by the voltage-dependent functions α and β (not given here) associated with each gating variable. $\phi = 3^{\frac{T-6.3}{10}}$, and alters the speed with which the gating variables respond to changes in cable potential. The equations for the Hodgkin-Huxley cable subject to a current ramp $I(t)$ injected at $x = 0$ are

$$\begin{aligned} C_m \frac{\partial V}{\partial t} &= \frac{d}{4R_i}\frac{\partial^2 V}{\partial x^2} - \bar{g}_{Na} m^3 h (V - E_{Na}) - \bar{g}_K n^4 (V - E_K) - g_L (V - E_L) && (4.11) \\ \frac{\partial m}{\partial t} &= \phi(\alpha_m(V)(1-m) - \beta_m(V)m) && (4.12) \\ \frac{\partial n}{\partial t} &= \phi(\alpha_n(V)(1-n) - \beta_n(V)n) && (4.13) \\ \frac{\partial h}{\partial t} &= \phi(\alpha_h(V)(1-h) - \beta_h(V)h), && (4.14) \end{aligned}$$

with boundary conditions

$$\begin{aligned} \frac{\partial V}{\partial x}(0,t) &= -\frac{4R_i}{\pi d^2} I(t) && (4.15) \\ \frac{\partial V}{\partial x}(L,t) &= 0. && (4.16) \end{aligned}$$

Here, L is the length of the cable in centimeters, and the current I is in μA. The compartmentalization of the system was as follows. Let the first compartment ($i = 1$) correspond to the end at which current is injected. For n compartments, the equations governing compartment i, $1 \leq i \leq n$, are

$$\begin{aligned} C_m \dot{V}_i &= -\bar{g}_{Na} m_i^3 h_i (V_i - E_{Na}) - \bar{g}_K n_i^4 (V_i - E_K) - g_L (V_i - E_L) \\ &+ \frac{(V_{i+1} - 2V_i + V_{i-1})}{R} && (4.17) \\ \dot{m}_i &= \phi(\alpha_m(V_i)(1-m_i) - \beta_m(V_i)m_i) && (4.18) \\ \dot{n}_i &= \phi(\alpha_n(V_i)(1-n_i) - \beta_n(V_i)n_i) && (4.19) \\ \dot{h}_i &= \phi(\alpha_h(V_i)(1-h_i) - \beta_h(V_i)h_i) && (4.20) \end{aligned}$$

where R is given by

$$R = \frac{4(\Delta x)^2}{d} R_i \tag{4.21}$$

and Δx is the length of one compartment. I define

$$V_0 = V_2 + \frac{2RI}{\pi d \Delta x} \tag{4.22}$$

$$V_{n+1} = V_{n-1} \tag{4.23}$$

to handle the boundary conditions.

Each compartment has associated with it four variables, the potential variable V and the three gating variables m, n, and h. Hence, for n compartments, the approximating ODE is $4n-$dimensional. For convenience when analyzing eigenvector components, I chose to arrange the equations such that for the $i'th$ compartment,

$$\dot{u_i} = x_i \tag{4.24}$$

$$\dot{m_i} = x_{i+n} \tag{4.25}$$

$$\dot{n_i} = x_{i+2n} \tag{4.26}$$

$$\dot{h_i} = x_{i+3n}. \tag{4.27}$$

The first n components of an eigenvector correspond to the potential in the cable, and components $n+1$ through $4n$ correspond to the gating variables. Except where noted otherwise, cable parameters were taken from Cooley and Dodge's 1966 paper [6]. In checking the WKB prediction against finite difference solutions of equations (4.11-4.16), I defined the observed I_j as the value

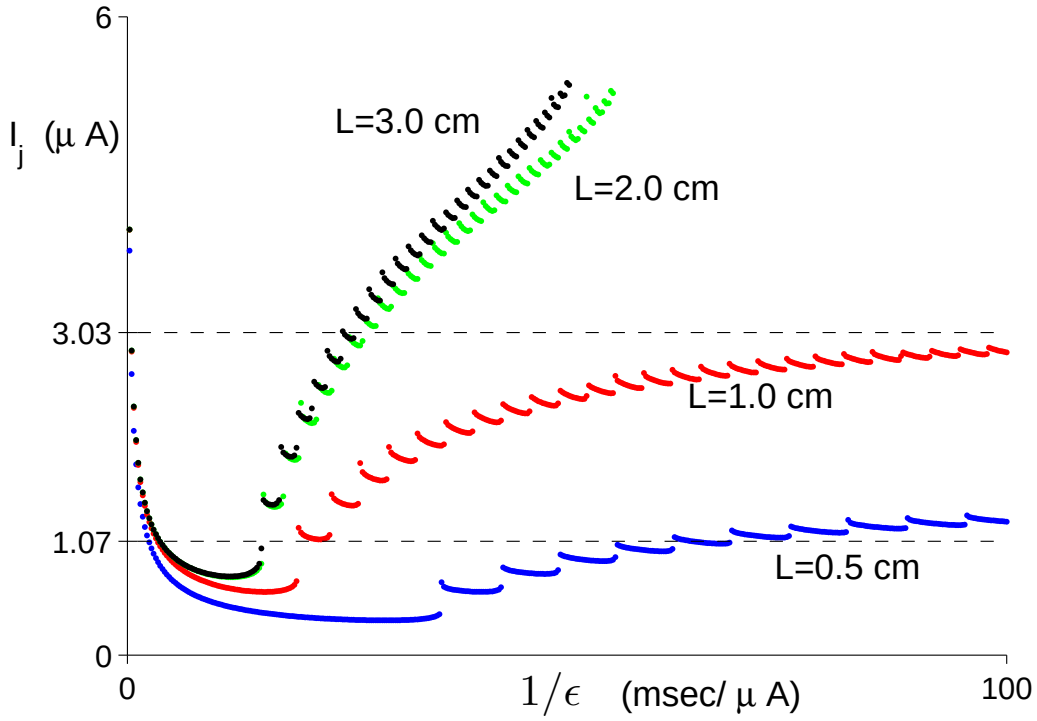

Figure 44: I_j observed in numerical solutions of the axonal cable PDE subject to the ramp $I(t) = \epsilon t$ versus inverse ramp speed, for Hodgkin-Huxley cables of several lengths at temperature 6.3 °C.

of injected current at the moment the potential at some point along the cable exceeds 40 mV.

I confirmed the phenomenon of complete accommodation for the Hodgkin-Huxley cable. Fig. 44 shows I_j versus the inverse ramp speed ϵ^{-1} obtained from numerical solutions for the cable lengths $L = 0.5$, $L = 1$, $L = 2$, and $L = 3$. The temperature was chosen to be 6.3°C.

As with the FitzHugh-Nagumo cable, the occurrence of complete accommodation for long but not short cables is due to the effect lengthening the cable has on the graph of $Re(\lambda(I))$. Integration of $Re(\lambda)$ versus I for various cable lengths indicates that the minimum length for complete accommodation

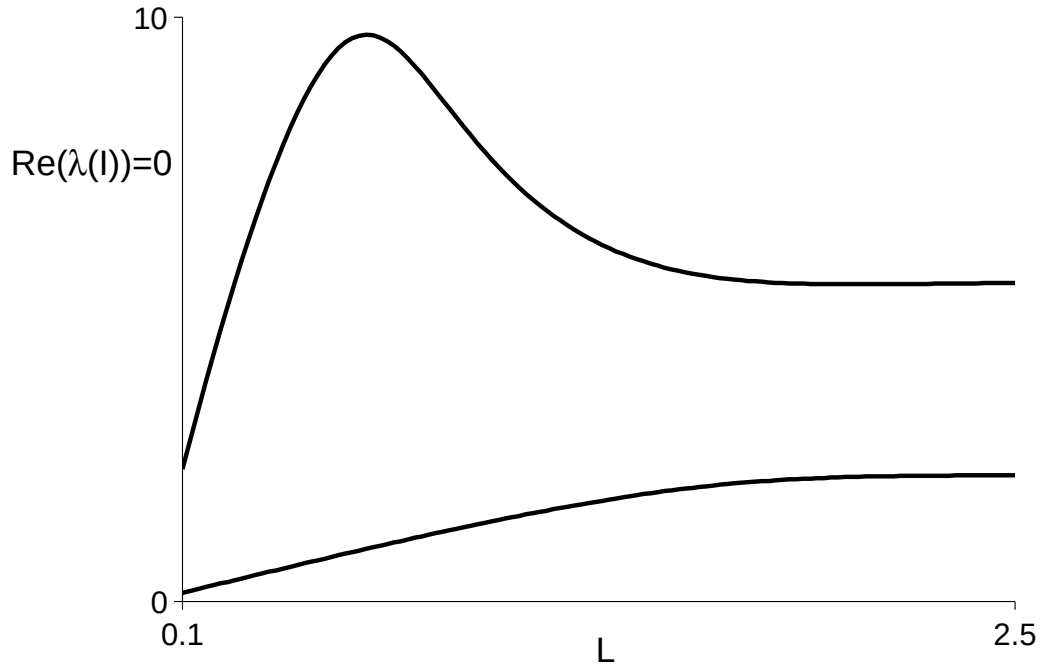

Figure 45: Plot of Hopf points versus cable length L, for a Hodgkin-Huxley cable at 6.3 °C.

in the Hodgkin-Huxley cable is approximately L_{min}= 1.45 cm for temperature 6.3°C. Fig. 45 plots the lower and upper Hopf points of the cable as a function of cable length; one can see that they approach limiting values as the cable length approaches infinity. Hence, no matter how long the cable is, there is always some excitable range of constant current I. Fig. 46 shows the same plot for the larger temperature 18.5°C. For the higher temperature, the Hopf points coalesce and vanish for large enough cable length; indeed, integration of $Re(\lambda)$ versus I indicates that the minimum length for complete accommodation of a linear current ramp from zero is about L_{min}=0.7 cm, significantly shorter.

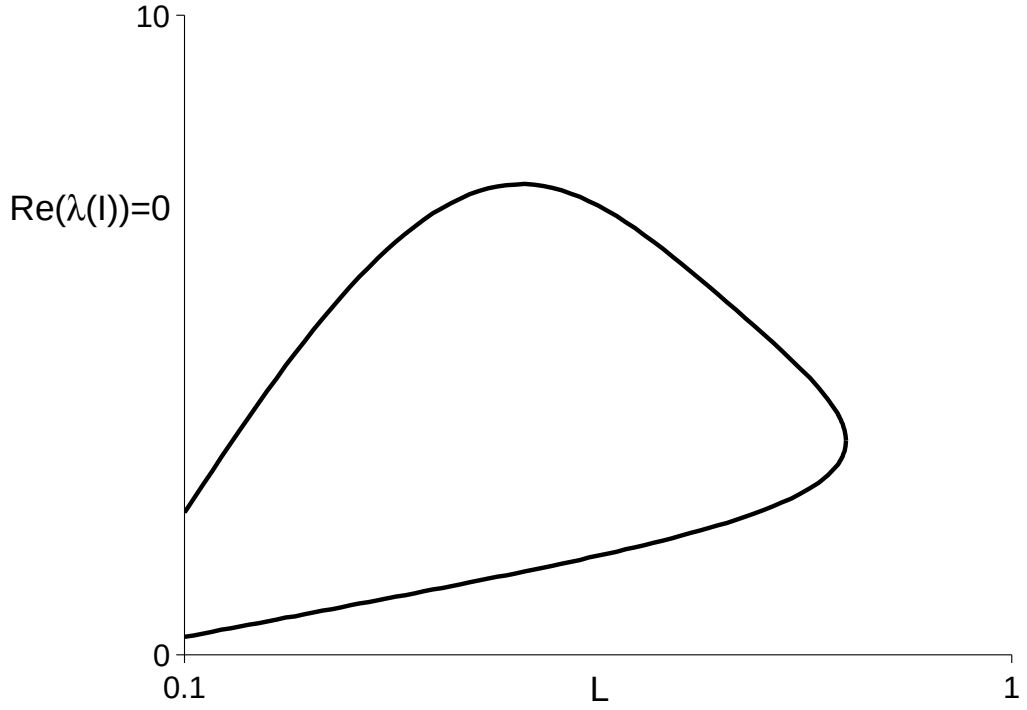

Figure 46: Plot of Hopf points versus cable length L, for a Hodgkin-Huxley cable at 18.5 °C.

4.4 Discussion

Comparison of responses of high-stem-conductance FitzHugh-Nagumo spiny dendritic cable and FitzHugh-Nagumo axonal cable to a slow current ramp

There are significant similarities between the responses of the FitzHugh-Nagumo spiny dendritic cable with uniform $G_{ss} = 0.35$ and the FitzHugh-Nagumo axonal cable to a slow current ramp. (1) There is one systemic Hopf bifurcation, caused by only one complex-conjugate eigenvalue pair crossing the imaginary axis. (2) At the onset of instability, significant oscillations in potential arise over a range of the cable; they are not highly localized as in the case of the spiny cable with $G_{ss} = 0.1$.

A spiny dendritic cable with a very high spine density ($\bar{n}$=120 was used, corresponding to 360 spines) and high stem conductance is similar to an axonal cable, in which the excitable channels are embedded in the cable shaft itself. However, there are differences. In the spiny cable with $G_{ss} = 0.35$ significant oscillations in the spinehead potential arise over the first quarter of the cable from the current-injection end, past which point they are insignificant in amplitude. In contrast, oscillations in potential arise all along the axonal cable shaft, with little attenuation as distance from the injection end increases. The WKB analysis yields the following insight: in the $G_{ss} = 0.35$ spiny cable, only one complex-conjugate eigenvalue pair attains positive real part (see Fig. 31); however, there are many complex-conjugate pairs with $Re(\lambda(I))$ having the same characteristic concave-down shape. Intuitively, even at this high value of stem conductance the spines still retain some of their independent character, and these complex eigenvalues with negative real part are mainly associated with the spines far from the injection point, in which significant oscillations do not arise. In contrast, for the FitzHugh-Nagumo (and the Hodgkin-Huxley) axonal cable, all eigenvalues are real except for a single complex-conjugate pair, which pair is responsible for the Hopf bifurcation. This indicates that the axonal cable behaves fully as a single system, which is to be expected as any compartments one wishes to view the cable as consisting of are directly coupled, in contrast to spines which are coupled diffusively via their spine stems.

Complete accommodation to a slow linear current ramp from $I_0 = 0$

For both the FitzHugh-Nagumo and Hodgkin-Huxley axonal cables, lengthening the cable stabilizes the system against oscillations provoked by a slow

current ramp in the sense that it reduces the real portion of the eigenvalue responsible for the onset of instability, which is integrated in computing the apparent firing threshold. This is not surprising, as external current is delivered only at one end of the cable, and as length increases the conductance load associated with the cable membrane increases. This reduction in the real portion of the eigenvalue governing stability with increasing cable length results in a minimum length for complete accommodation in response to a slow linear current ramp from $I_0 = 0$, for both the FitzHugh-Nagumo and Hodgkin-Huxley cables.

Whether the stabilizing effect of lengthening the cable eventually saturates (the two Hopf points asymptote as $L \to \infty$) or not (the two Hopf points coalesce and disappear for some value of L) can be intuitively viewed as a competition between the stabilizing effect of additional membrane load and the destabilizing effect of additional ion channels embedded in the membrane. For the Hodgkin-Huxley cable at temperature 6.3 °C, the Hopf points continue to exist and approach limiting values as $L \to \infty$; hence, there is always an excitable range of constant current (although a slow current ramp $I(t) = \epsilon t$ fails to provoke firing beyond a certain length). For the Hodgkin-Huxley cable at temperature 18.5 °C, there is a length beyond which the two Hopf points coalesce: not even a constant injected current I, of any value, can provoke the cable to fire. Furthermore, the minimum length for complete accommodation of the current $I(t) = \epsilon t$ is much shorter for the higher temperature.

One can understand the stabilizing effect of increased temperature on the Hodgkin-Huxley cable by noting that temperature only impacts the dynamics via the parameter ϕ multiplying the gating variables. For the temperature of 18.5 °C, ϕ is extremely large and the gating variables are practically at their

steady-state values dictated by the instantaneous potential V. Hence, there is very little time lag in the response of the gating variables to the potential; in terms of the physical nerve cell being modeled, this means that the sodium current flows into the membrane for very little time before its channels close, and the potassium current quickly responds to bring the voltage down again. Both of these factors stabilize the system against action potentials.

Chapter 5

DISCUSSION AND FUTURE DIRECTIONS

5.1 Summary of findings

I have investigated dynamic Hopf bifurcation in spatially-extended excitable systems using models from neuroscience. The two systems considered were the spiny cable, modeling a passive dendritic shaft studded with excitable spines, and axonal cables, modeling a nerve fiber in which the ion channels responsible for excitability are embedded in the shaft itself, such as an unmyelinated axon. For simplicity, I have focused on FitzHugh-Nagumo dynamics, although I did examine the phenomenon of complete accommodation to a slow linear current ramp from $I_0 = 0$ in the Hodgkin-Huxley axonal cable. In all cases, the slowly rising current ramp was applied by injecting it into one end of the cable while the other end was sealed to current. In order to predict the apparent firing threshold I_j in response to a slow current ramp, I applied the WKB method to the approximating ODE obtained from viewing the cable as consisting of a large number of isopotential compartments. I discovered that the WKB method also provides a prediction of the location along the cable at which the largest-amplitude oscillations in membrane potential arise (spinehead membrane potential for the spiny cable, cable shaft membrane potential for the axonal cable) once $I(t) = I_j$. All WKB predictions were compared with numerical solutions of the PDE model, executed in quadruple precision arithmetic.

I investigated a model of a spiny dendritic cable in which 75 excitable spines are uniformly distributed on a passive shaft of length $L = 3$, with uniform stem conductances. For the intermediate stem conductance $G_{ss} = 0.1$, I found that

slow current ramps provoke oscillations which, although small in amplitude, are still significant and are highly localized at a point on the cable distal from the site of current injection. At first glance this appears counterintuitive. However, one can see why this is by considering the results for the case of very low stem conductance, $G_{ss} = 0.02$. Each of the 75 complex-conjugate pairs of eigenvalues, whose real portions are plotted in Fig. 21, was found to be primarily associated with one spine for I throughout the range considered, as indicated by an inspection of the associated eigenvectors. For each spine, the real portion of the complex-conjugate eigenvalue pair crosses the $I-$axis twice, at I_L and I_U Here one approaches a situation in which the spines are decoupled, each having its own interval of injected current $[I_L, I_U]$ over which it fires; for spines further from the injection point, I_L and I_U are larger and the interval $[I_L, I_U]$ wider due to leakage losses through the passive shaft and the current that is diverted by spines nearer the injection point.

I found that when G_{ss} is increased to 0.1, a dominant eigenvalue pair arises which is responsible for satisfying the onset condition in response to a slow current ramp (Fig. 24). An inspection of the components of one of the eigenvectors $\vec{v}_j$ associated with this dominant pair indicates that it effects potential oscillations away from the slowly-varying solution in all spineheads. However, the identity of the spine for which the oscillations are largest in amplitude shifts away from the injection point as I_j increases, indicating that information about the individual firing ranges each spine would possess if coupling with other spines were negligible is contained in $\vec{v}_j$. By manipulating the current ramp used (initial condition and/or functional form of the ramp) I can select I_j and hence select the location along the cable at which oscillations would arise.

The WKB method suggests that no slow current ramp can give rise to distal oscillations in spinehead potential for the very low stem conductance of $G_{ss} = 0.02$, because the eigenvalue which would first satisfy the onset condition is associated with the spine at the current-injection end for all I. In the spiny cable with large stem conductance $G_{ss} = 0.35$ and the axonal cable, oscillations are predicted to be highly delocalized, and this was confirmed with numerical solutions. This suggests that in order for a slow current ramp injected at one end of a cable to give rise to localized distal oscillations in potential, (1) the ion channels responsible for excitability must be isolated in spineheads rather than embedded in the shaft membrane, and (2) an intermediate value of spine stem conductance is required.

I have shown that a slow current ramp injected at one end of a spiny dendritic cable can provoke localized distal oscillations in the spinehead membrane potential, even when all geometric and electrical parameters, as well as the distribution of ion channels, are uniform. The effect is even easier to get if one has the more physically realistic situation of nonuniform spine stem conductances, as shown in chapter two. The results of chapter two suggest that for a continuous distribution of spines (uniform or not), distal oscillations in spinehead membrane potential can be provoked even by a ramp with initial current very close to the first Hopf point, if the distal spines have large enough stem conductances. Although the geometry of the system dictates a natural firing order for the spines, it is easily overcome by the effect of differing stem conductances.

Another physically realistic feature which might result in distal oscillations in spinehead membrane potential is a nonuniform distribution of spines along the cable (nonuniform spine density). When stem conductance and spine

density are uniform, increasing the number of spines on the cable increases the two current values at which Hopf points occur; this is because the current coming down the shaft is now divided among more spines. Although I did not make a study of it, this suggests that decreasing the spine density at a given point along the cable may have an effect similar to increasing the stem conductance there, and cause such sparse patches to fire first in response to current ramps starting close to the first Hopf point. Future work will have to determine whether this is the case. I note that any nonuniformity in the system may be introduced without complicating the WKB compartmental analysis; indeed, it even applies to systems which cannot be written as a simple ordinary or partial differential equation.

5.2 Remarks on boundary conditions

In this dissertation I have assumed that one end of the cable is sealed to current, and the other end is injected with a slowly-rising current ramp. One could have considered other boundary conditions; for example, rather than sealing the far end to current, one could fix its potential at $V = 0$. For long cables one would not expect this to make much difference, as little current reaches the far end. One interesting alternative boundary condition would be to replace the slowly-rising injected current with a slowly-rising command potential $V(\epsilon t)$. This could describe a cable attached to an active soma whose potential is slowly rising. If different boundary conditions were used but the problem remained such that (1) at each point along the cable, the potential in the shaft increased slowly with time and (2) at each moment of time, the potential in the shaft decreased monotonically from the stimulus end, I speculate that similar qualitative results would be obtained; this was the situation

in the cable shaft for the boundary conditions considered. In particular, I speculate that the nonlocal effect would be preserved for the spiny cable with intermediate stem conductance.

5.3 Possible applications and directions for future work

I emphasize that although I have demonstrated the interesting nonlocal effect for systems taken from neuroscience, the conditions for it to occur are very general. This effect could arise in any reaction-diffusion system experiencing a slowly ramped parameter p in which (1) there is some degree of decoupling between the reactive and diffusive portions of the system, (2) in the limit that they become decoupled, each reactive element undergoes two Hopf bifurcations with respect to p and hence has an "excitable range." In general, the differing physical locations of the reactive elements will result in differences in their excitable ranges of p, which makes the nonlocal effect possible. I now consider two physiological systems in which the nonlocal effect might arise.

Slow-rising synaptic currents into the dendritic shaft

NMDA receptors embedded in the dendritic shaft provide a possible scenario by which a segment of spiny dendritic cable might encounter a slowly-rising injected current. NMDA channels open in response to glutamate, the primary excitatory neurotransmitter, and give rise to an excitatory post-synaptic current with a slow rise-time and decay of several hundred milliseconds [19]; in contrast, the time course of an action potential is a few milliseconds. There is great morphological variance among dendritic spines, and an accompanying wide range of stem resistances, which are estimated to range from 10^7 to $10^{10}\Omega$ [23]. As was seen in chapter two, the stem conductance (inverse of resistance) has a profound impact on which spine fires first in response to a

slowly rising current, and can easily cause spines distal from the site of current injection to fire first, bypassing spines physically closer to the injection site. This may play a role in the computational properties of the dendritic process.

Pain and ectopic firing

Distal initiation of oscillations were not observed in the axonal cable, which models a structure such as an unmyelinated axon. However, in a myelinated axon the excitable components are the nodes of Ranvier, separated from each other by myelinated segments which act as resistors [15]. This segregation of the reactive and diffusive elements of the system might enable the interesting phenomenon of distal initiation of firing in response to a slow current ramp to arise.

Pseudounipolar neurons, such as dorsal root ganglion neurons, have no dendrites and instead have an axon with two branches, the peripheral branch and the central branch [13]. At the end of the peripheral branch are sensory receptors, stimulation of which causes a signal to be conducted down the axon, past the cell body, and ultimately to the spinal cord. The natural stimuli likely to be experienced by dorsal root ganglion neurons are well modeled as slow current ramps [16], making DRG cells a potential application of the results outlined here. In addition, the generation of action potentials at abnormal locations ("ectopic firing") which is seen in damaged dorsal root ganglion cells has been implicated in neuropathic pain [16].

REFERENCES

[1] S.M. Baer, T. Erneux, and J. Rinzel. The slow passage through a Hopf bifurcation: Delay, memory effects, and resonance. *SIAM Journal on Applied Mathematics*, 49:55–71, 1989.

[2] S.M. Baer and E.M. Gaekel. Slow acceleration and deacceleration through a Hopf bifurcation: Power ramps, target nucleation, and elliptic bursting. *Physical Review E*, 78(036205), 2008.

[3] S.M. Baer and J. Rinzel. Propagation of dendritic spikes mediated by excitable spines: A continuum theory. *Journal of Neurophysiology*, 65:874–890, 1991.

[4] C. Bender and S. Orszag. *Advanced Mathematical Methods for Scientists and Engineers: Asymptotic Methods and Perturbation Theory.* Springer, 1999.

[5] P.L. Chen and J. Bell. Spine-density dependence of the qualitative behavior of a model of a nerve fiber with excitable spines. *Journal of Mathematical Analysis and Applications*, 187:384–410, 1994.

[6] J.W. Cooley and F.A. Dodge. Digital computer solutions for excitation and propagation of nerve impulse. *Biophysical Journal*, 6:583–599, 1966.

[7] E. du Bois-Reymond. *Untersuchungen ueber thierische Elektricitaet.* G. Reimer, 1849.

[8] B. Ermentrout and D. Terman. *Mathematical Foundations of Neuroscience.* Springer, 2010.

[9] R. FitzHugh. Impulses and physiological states in theoretical models of nerve membrane. *Biophysical Journal*, 1:445–466, 1961.

[10] H.M Hastings, R.J. Field, and S.G. Sobel. Microscopic fluctuations and pattern formation in a supercritical oscillatory chemical system. *Journal of Chemical Physics*, 119:3291–3296, 2003.

[11] A.L. Hodgkin and A.F. Huxley. A quantitative description of membrane current and its application to conduction and excitation in nerve. *Journal of Physiology-London*, 117:500–544, 1952.

[12] E. Jakobsson and R. Guttman. The standard Hodgkin-Huxley model and squid axons in reduced external C^{++} fail to accommodate to slowly rising currents. *Biophysical Journal*, 31:293–298, 1980.

[13] E. Kandel, J. Schwartz, and T. Jessell. *Principles of neural science.* McGraw-Hill, fourth edition, 2000.

[14] S. Karimov. Asymptotics of solutions of some classes of differential equations with a small parameter multiplying derivatives, when there is a change of stability of a stationary point in the fast motion plane. *Differential Equations*, 21:1136–1139, 1985.

[15] J. Keener and J. Sneyd. *Mathematical Physiology.* Springer, 1998.

[16] Y. Kovalsky, R. Amir, and M. Devor. Subthreshold oscillations facilitate neuropathic spike discharge by overcoming membrane accommodation. *Experimental Neurology*, 210:194–206, 2008.

[17] R. Kuske. Probability densities for noisy delay bifurcations. *Journal of Statistical Physics*, 96:797–816, 1999.

[18] R. Kuske and S.M. Baer. Asymptotic analysis of noise sensitivity in a neuronal burster. *Bulletin of Mathematical Biology*, 64:447–481, 2002.

[19] R.A.J. Lester, J.D. Clements, G.L. Westbrook, and C.E. Jahr. Channel kinetics determine the time course of NMDA receptor-mediated synaptic currents. *Nature*, 346:565–567, 1990.

[20] A.I. Neishtadt. Persistence of stability loss for dynamical bifurcations I. *Differential Equations*, 23:1385–1391, 1987.

[21] W. Nernst. Zur Theorie des electrischen Reizes. *Pfluegers Archiv fuer die gesamte Physiologie des Menschen und der Tiere*, 122:275–314, 1908.

[22] J. Rinzel and S.M. Baer. Threshold for repetitive activity for a slow stimulus ramp. *Biophysical Journal*, 54:551–555, 1988.

[23] I. Segev and W. Rall. Computational study of an excitable dendritic spine. *Journal of Neurophysiology*, 60:499–523, 1988.

[24] S.G. Sobel, H.M. Hastings, and R.J. Field. Oxidation state of BZ reaction mixtures. *Journal of Physical Chemistry A*, 110:5–7, 2006.

[25] J. Su. On delayed oscillation in nonspatially uniform Fitzhugh-Nagumo equation. *Journal of Differential Equations*, 110:38–52, 1994.

[26] J.Z. Su, J. Rubin, and D. Terman. Effects of noise on elliptic bursters. *Nonlinearity*, 17:133–157, 2004.

[27] T. Tateno, A. Harsch, and H.P.C. Robinson. Threshold firing frequency-Current relationships of neurons in rat somatosensory cortex: type 1 and type 2 dynamics. *Journal of Neurophysiology*, 92:2283–2294, 2004.

[28] A.B. Vallbo. Accommodation related to inactivation of sodium permeability in single myelinated nerve fibres from Xenopus Laevis. *Acta Physiologica Scandinavica*, 61:429–444, 1964.

[29] D.W. Verzi, M.B. Rheuben, and S.M. Baer. Impact of time-dependent changes in spine density and spine shape on the input-output properties of a dendritic branch: A computational study. *Journal of Neurophysiology*, 93:2073–2089, 2005.

[30] H.Y. Wu and S.M. Baer. Analysis of an excitable dendritic spine with an activity-dependent stem conductance. *Journal of Mathematical Biology*, 36:569–592, 1998.

[31] K. Zaremba. Relaxation oscillators and bursters coupled to passive cables. Master's thesis, Arizona State University, Tempe, AZ, 1998. Chapter 2.

[32] Y. Zhou. Unique wavefront for dendritic spines with Nagumo dynamics. *Mathematical Biosciences*, 148:205–225, 1998.

APPENDIX A

DERIVATION OF ONSET CONDITION

A very simple, highly idealized model of an excitable cell is provided by the FitzHugh-Nagumo system of equations. This a two-dimensional ODE system which captures some of the qualitative features of the more realistic Hodgkin-Huxley system while remaining analytically tractable. Its two variables are u and w, where u represents membrane potential and w is a slow recovery variable which acts to restore u to its resting value of zero after an action potential; hence, w serves the same purpose as the potassium current in the Hodgkin-Huxley system. I represents injected current.

$$\dot{u} = -f(u) - w + I \tag{1}$$

$$\dot{w} = b(u - \gamma w) \tag{2}$$

Here, $f(u) = u(u-a)(u-1)$; this term is responsible for the threshold behavior of the model, which is accomplished via the sodium current in the Hodgkin-Huxley model. Let $a = 0.1$, $b = 0.05$, and $\gamma = 1$. For these parameters, the system has a unique steady state $(u_{ss}(I), w_{ss}(I))$ for all values of I, and the system undergoes a supercritical bifurcation at the two Hopf points.

I switch to the vector form of the system and denote the steady state by $\overrightarrow{x_{ss}}(I)$. To determine the stability of $\overrightarrow{x_{ss}}(I)$ one must linearize the system about the steady state. So long as the Jacobian $\mathbf{J}$ of the system evaluated at the steady state is nonsingular, the behavior of small deviations from $\overrightarrow{x_{ss}}(I)$ under the linear system will be qualitatively equivalent to their behavior under the full system.

$$\mathbf{J}(\overrightarrow{x_{ss}}(I)) = \begin{bmatrix} -3u_{ss}^2 + 2(a+1)u_{ss} - a & 1 \\ b & -b\gamma \end{bmatrix}$$

The eigenvalues of the above matrix determine the local stability of $\overrightarrow{x_{ss}}(I)$. Since the current I appears additively in the equations, it falls out of the linearization. However, it impacts the Jacobian indirectly through its determination of the point $\overrightarrow{x_{ss}}(I)$ at which the Jacobian is evaluated. To emphasize this dependence, I write $\mathbf{J}(I)$.

Hence, each value of I determines a set of eigenvalues governing the local stability of the steady state $\overrightarrow{x_{ss}}(I)$. The FitzHugh-Nagumo model with the chosen parameters undergoes two supercritical Hopf bifurcations at I_1 and I_2, $0 < I_1 < I_2$. In particular: for $I < I_1$, the two eigenvalues lie in the left open half of the complex plane. For I in (I_1, I_2) there is one complex conjugate pair of eigenvalues with positive real part. For $I > I_2$ the two eigenvalues again lie in the left open half-plane. When the eigenvalues cross the imaginary axis at the Hopf points, they do so transversally, that is, $\frac{dRe[\lambda(I_1)]}{dI} > 0$ and $\frac{dRe[\lambda(I_2)]}{dI} < 0$. Finally, $Im[\lambda(I_1)] \neq 0$ and $Im[\lambda(I_2)] \neq 0$, that is, the Hopf bifurcations are nondegenerate.

Now consider the situation in which I is not static but rather is a slowly-varying function of time. For the moment consider a "slow linear ramp," in which I increases linearly from initial value $I_0 < I_1$ at a very slow rate $0 < \epsilon \ll 1$, called the ramp speed. The model is

$$\dot{u} = -f(u) - w + I(\epsilon t) \tag{3}$$

$$\dot{w} = b(u - \gamma w) \tag{4}$$

I switch to the slow time variable $\tau = \epsilon t$ and rewrite the system. By the prime symbol I denote differentiation with respect to the slow time variable

τ. Defining $U(\tau) = u(t)$ and $W(\tau) = w(t)$, the system becomes

$$\epsilon U' = -f(U) - W + I \tag{5}$$

$$\epsilon W' = b(U - \gamma W) \tag{6}$$

$$I' = 1. \tag{7}$$

Writing the system in this form, one sees that this system is actually a singular perturbation of the system with static I. In the parlance of multiple-scale methods, the equations governing $\overrightarrow{X}(\tau) = (U(\tau), W(\tau))$ constitute the fast subsystem while the equation governing the current is the slow subsystem.

Recall that for the case of static parameter I, the system's steady state was given by the function $\overrightarrow{x_{ss}}(I)$. For the perturbed system, the function $\overrightarrow{x_{ss}}(I(\tau))$ constitutes the quasi-static solution. It is not a true solution to the problem for nonzero ϵ: since I varies with τ, so too do the values of U and W given by $\overrightarrow{x_{ss}}(I)$, but those values are precisely the ones which cause U' and W' to be zero. Hence, $\overrightarrow{x_{ss}}(I(\tau))$ does not satisfy the perturbed differential equation. However, singular perturbation theory for dynamical systems ensures that for small enough ϵ, there will be a true solution to the system which closely tracks the quasi-static solution [14, 20]. I denote this solution by $\overrightarrow{x_{sv}}(\tau)$, where "sv" stands for "slowly varying." It is slowly varying because it evolves on the slow time scale τ. For the case of static current, one needed to determine the behavior of deviations from the steady state $\overrightarrow{x_{ss}}(I)$. Here, one must determine the behavior of deviations from $\overrightarrow{x_{sv}}(\tau)$. To do this, one linearizes about $\overrightarrow{x_{sv}}(\tau)$. Switching to vector form, the system linearized about $\overrightarrow{x_{sv}}(\tau)$ is

$$\epsilon \overrightarrow{X}' = \mathbf{J}(\overrightarrow{x_{sv}}(\tau))\overrightarrow{X} \tag{8}$$

where $\overrightarrow{X}(\tau)$ represents a deviation from $\overrightarrow{x_{sv}}(\tau)$. If b and γ are $O(1)$, an inspection of the equations for U' and W' indicates that $\overrightarrow{x_{sv}}(\tau)$ must be ϵ away from the curve $\overrightarrow{x_{ss}}(\tau)$; this follows from the fact that $\overrightarrow{x_{sv}}(\tau)$ varies as $O(1)$ on the τ time scale.

In general, one cannot obtain an explicit formula for $\overrightarrow{x_{sv}}(\tau)$. However, one may write the following regular perturbation expansion for it [1, 2, 22]:

$$\overrightarrow{x_{sv}}(\tau) \sim \overrightarrow{x_{ss}}(I(\tau)) + \epsilon\overrightarrow{x_1}(\tau) + ... \tag{9}$$

as $\epsilon \to 0$. The $\overrightarrow{x_i}(\tau)$ are unknown functions. Since $\mathbf{J}(\overrightarrow{x_{sv}}(\tau)) \sim \mathbf{J}(\overrightarrow{x_{ss}}(I(\tau)))$ as $\epsilon \to 0$, the qualitative behavior of deviations from $\overrightarrow{x_{sv}}(\tau)$ is given by

$$\epsilon\overrightarrow{X}' = \mathbf{J}(\overrightarrow{x_{ss}}(I(\tau)))\overrightarrow{X} \tag{10}$$

for small enough $\epsilon > 0$. This is a linear homogeneous equation with slowly-varying coefficients. An approximate analytic solution for such problems can be obtained via the WKB method [4], which assumes that there is scalar function $\sigma(\tau)$ and vector functions $\overrightarrow{X_i}(\tau)$ such that

$$\overrightarrow{X}(\tau;\epsilon) \sim e^{\frac{\sigma(\tau)}{\epsilon}}\left[\overrightarrow{X_0}(\tau) + \epsilon\overrightarrow{X_1}(\tau) + ...\right] \tag{11}$$

as $\epsilon \to 0$.

Substituting this expansion into the equation and solving for the leading-order term, one obtains the algebraic problem

$$[\mathbf{J} - \sigma'(\tau)\mathbf{I}]\overrightarrow{X_0}(\tau) = \overrightarrow{0} \tag{12}$$

where by assumption $\overrightarrow{X_0}(\tau) \neq \overrightarrow{0}$. One sees from this equation that $\overrightarrow{X_0}(\tau)$ is an eigenvector $\overrightarrow{v}(\tau)$ of $\mathbf{J}(\overrightarrow{x_{ss}}(I(\tau))$ with corresponding eigenvalue $\lambda(\tau) = \sigma'(\tau)$.

A fundamental solution to leading order is then

$$\overrightarrow{X}(\tau) \sim e^{\frac{1}{\epsilon}\int_0^\tau \lambda(I(\tau))d\tau}\ \overrightarrow{v}\left(I(\tau)\right). \tag{13}$$

The motivation behind the WKB expansion can be understood by considering that for the scalar differential equation $\epsilon x' = f(\tau)x$, the solution (up to an arbitrary multiplicative constant) is given by $x(\tau) = e^{\frac{1}{\epsilon}\int_0^\tau f(s)ds}$. For a first-order system of equations $\epsilon\overrightarrow{X}' = \mathbf{F}(\tau)\overrightarrow{X}$ the analogous formula is $\overrightarrow{X}(\tau) = e^{\frac{1}{\epsilon}\int_0^\tau \lambda(s)ds}\overrightarrow{V}(\tau)$, where $\lambda(\tau)$ is an eigenvalue of $\mathbf{F}(\tau)$ with corresponding eigenvector $\overrightarrow{V}(\tau)$. Because of the time derivative of the eigenvector, this is not a solution to the problem, however, it satisfies it asymptotically as $\epsilon \to 0$ and hence gives the solution to leading order. Higher-order corrections are obtained by solving for the vector functions $\overrightarrow{X}_i$, $i = 1, 2, ...$

For the FitzHugh-Nagumo system, there are two (up to multiplication by nonzero complex conjugate constants) fundamental solutions. For an ODE in n variables, there are n fundamental solutions, one for each eigenpair of the Jacobian. A given fundamental solution becomes $O(1)$ away from $\overrightarrow{x_{sv}}(\tau)$ at the smallest $\tau > 0$ satisfying

$$\int_0^\tau Re\left[\lambda(I(\tau))\right] d\tau = O(\epsilon) \tag{14}$$

which for simplicity is approximated in this dissertation as

$$\int_0^\tau Re\left[\lambda(I(\tau))\right] d\tau = 0. \tag{15}$$

The general solution to (10) is a linear combination of the fundamental solutions. Hence, it follows that the slowly-varying solution $\overrightarrow{x_{sv}}(\tau)$ becomes unstable at the smallest value of $\tau > 0$ such that, for some $1 \leq i \leq n$,

$$\int_0^{\tau} Re\left[\lambda_i(I(\tau))\right] d\tau = 0. \tag{16}$$

For a linear ramp, $I(\tau) = I_0 + \tau$, one can replace (16) with

$$\int_{I_0}^{I} Re\left(\lambda_i(I)\right) dI = 0. \tag{17}$$

In contrast to the case of constant bifurcation parameter I, the slowly-varying solution is not predicted to lose stability the moment I attains the value I_1. Rather, it is predicted to remain stable until a value of I is reached such that one of the eigenvalues λ_i satisfies the above integral. When this happens, the fundamental solution associated with that eigenvalue has "wound away" from the slowly-varying solution as far as it "wound in" towards it while λ_i had negative real part. I denote the smallest value of $I > I_0$ for which (17) is satisfied for some $1 \leq i \leq n$ as I_j. Hence, I_j is the WKB prediction for the onset of instability.

I note that I_j exceeds the first Hopf point I_1 by a finite value as $\epsilon \to 0$. That is, as $\epsilon \to 0$, one does not recover the static current behavior. This arises from the fact that (8) is a singular perturbation problem. In general, to determine I_j one must keep track of $\int_{I_0}^{I} Re(\lambda_i(I))dI$ for each of the eigenvalues. For the simple FHN model both integrals will be the same because the eigenvalues are a complex conjugate pair. In contrast to the case for static I, one cannot speak simply of the stability or instability of the slowly-varying solution. The current at which the system becomes unstable depends on the initial current I_0 when the ramp began. One must keep in mind that there is no unqualified I_j for the onset of sustained oscillations: I_j is a function of I_0.